Medizinische Fakultät
der
Universität Duisburg-Essen

Aus dem Augenzentrum am St. Franziskus-Hospital Münster

Influence of TSP-1/CD47 Signaling in Trabecular Meshwork Cells after Elevated Hydrostatic Pressure *in Vitro*

I n a u g u r a l d i s s e r t a t i o n
zur
Erlangung des Doktorgrades der Medizin
durch die Medizinische Fakultät
der Universität Duisburg-Essen

Vorgelegt von
Xiaoyu Wu
aus Guizhou P.R.China
2024

DOI: 10.17185/duepublico/82199
URN: urn:nbn:de:hbz:465-20240801-094553-7

Dekan: Herr Univ.-Prof. Dr. med. J. Buer

1. Gutachter: Herr Prof. Dr. med. C. Heinz

2. Gutachter: Herr Priv.-Doz. Dr. med. T. Hudde

Tag der mündlichen Prüfung: 7. Juni 2024

1 Introduction

1.1 The human eye and the anterior chamber

The human eye is the primary organ for vision in humans and is composed of various components. Although the eyeball is not a perfect sphere, it has a quasi-spherical structure due to the more curved cornea. The eye consists of the anterior segment, which includes the cornea, anterior chamber, iris, lens, and ciliary body, as well as the posterior segment. The posterior segment, which makes up the back two-thirds of the eyeball, encompasses the vitreous, choroid, retina and optic nerve. The cornea serves as the transparent tissue and the first opening where the light enters the eye. Diminished corneal transparency can lead to visual impairment. The cornea connects to the sclera through a structure called corneal limbus. It serves as the outermost layer of eyeball known as the fibrous tunic and provides support for the eyeball shape whilst safeguarding the internal eye structure. The vascular tunic or uvea, which contains the choroid, ciliary body and iris, forms the secondary layer. The retina, the innermost layer of the eye, is light sensitive and transforms images into electrical nerve impulses for the brain to allow visual perception. The anterior chamber (AC) is the front part of the eye located between the cornea and iris. It is filled with aqueous humor (AH) which supplies necessary nutrients to the surrounding tissues and plays a crucial role in maintaining normal intraocular pressure (IOP) (Tamm, 2009). The AC is an angular cavity anteriorly formed by the endothelium of the cornea and posteriorly by the lens within the pupillary aperture, the anterior surface of the iris, and part of the ciliary body. The AC angle is the angle between the iris and corneal endothelium. The Schwalbe's line marks the anterior surface of the anterior wall of the angle, which is the end of corneal Descemet's membrane. The anterior wall is terminated by the scleral spur, with the unpigmented and pigmented meshwork (the pathway of AH) in between. The iris root forms the posterior wall, and the anterior surface of the ciliary body known as ciliary band (a grey or dark brown band) forms the recess. The degree of AC angle plays a crucial role in the diagnosis, classification, treatment, and prevention of various types of glaucoma.

1.2 Production and outflow of aqueous humor in the healthy eye

In a healthy eye, the normal IOP ranges between 10 to 21mmHg, and the balance between the formation and outflow of AH maintains a stable IOP (Doughty and Zaman, 2000). A balanced IOP is crucial to maintain ocular health.

The volume of AH is usually regulated to manage IOP. The ciliary body produces AH, which then flows through the pupil into the AC. There are two pathways for AH outflow: the trabecular outflow pathway (conventional outflow), which accounts for 80% of AH outflow, and the uveoscleral outflow pathway (unconventional outflow), accounting for 20%. In the conventional pathway, the AH flows through the trabecular meshwork, then traverses the juxtacanalicular connective tissue, enters Schlemm's canal, then the collecting channels, and finally the episcleral venous system. The AH outflow in the unconventional pathway traverses the ciliary band of the AC angle, then passes into the ciliary muscle gap, followed by entry into the suprachoroidal space, and ultimately exits through the sclera into the orbital vessels. The second pathway is modulated by inflammatory cytokines during inflammation and is also augmented by antiglaucomatous prostaglandin therapy. Some researchers have suggested that AH likely passes through the vitreous humor and on through the retinal pigment epithelium (RPE) in order to reach the choroidal vessels (Smith et al., 2020).

1.3 Trabecular meshwork

The trabecular meshwork (TM) is a tissue located at the AC angle of the eye, exhibiting a sieve-like structure. The TM comprises four regions of the TM (from inner to outermost) and can be segregated into two functional segments: (1) The uveal meshwork is the innermost layer adjacent to the anterior chamber and comprises of a network of collagen and elastin lamellae covered by TM cells; (2) The corneoscleral meshwork constitute the intermediate layer and comprises a series of perforated collagen and elastin plates, covered by TM cells; (3) The outermost layer, called the juxtacanalicular layer, is composed loose and unstratified connective tissue containing TM cells. These cells are

surrounded by extracellular matrix (ECM) and arranged in a network; (4) The last layer, which is distinct from the previous three layers and considered the “filtering” TM, is located below the Schwalbe’s line in the "non-filtering" region or insert region (Vingolo et al., 2019). The inner three parts form a part that communicates with SC and is called “filtering”. The outer insert region contains TM stem cells, according to the literature (Tamm, 2009). Several hypotheses suggest that this region acts as a reservoir for dividing and relocating cells to the filtering TM after injury (Yun et al., 2016). Figure 1 illustrates the structure of the human trabecular meshwork and its outflow pathways.

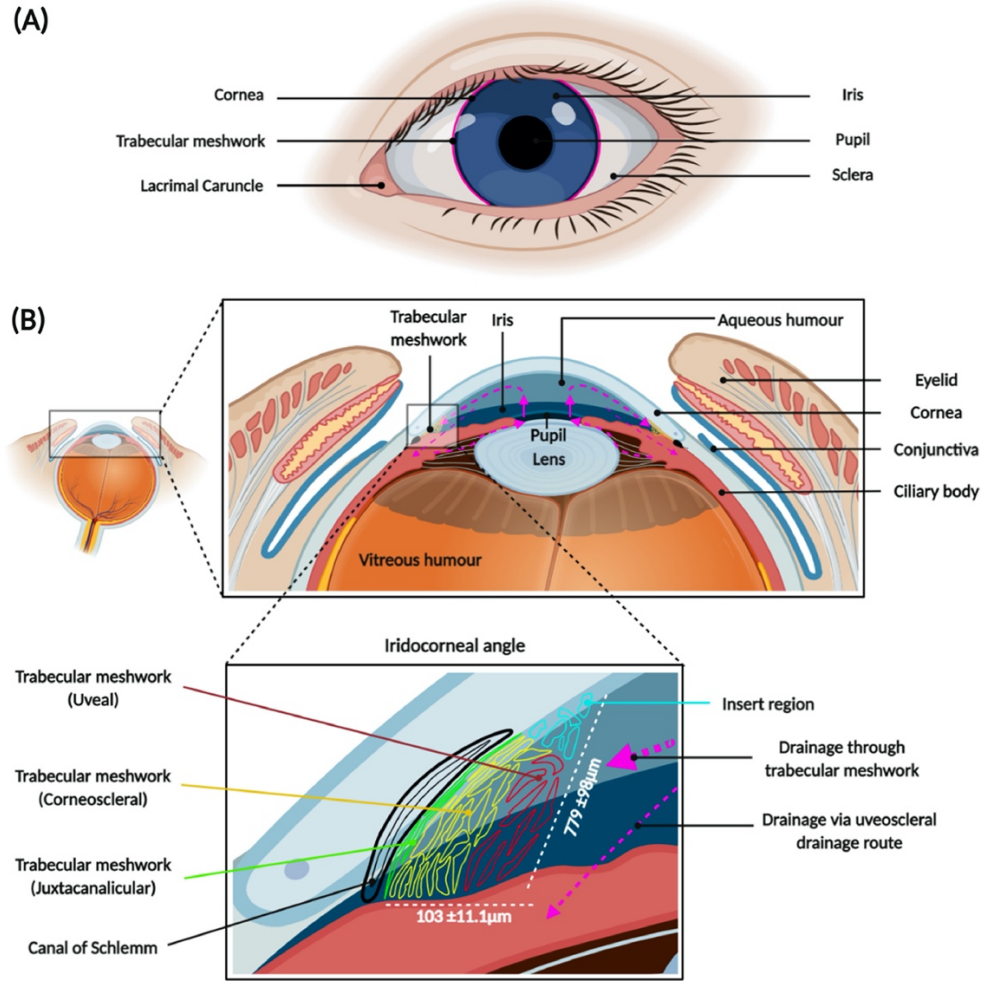

Figure 1. The structure of the human eye.
(A) The pink circle shows the location of trabecular meshwork. (B) The anterior segment of the eye. Pink arrows show the flow directions. (Crouch et al., 2021)

TM cells comprise three functional cell types: endothelial cells, myofibroblasts and macrophages (Stamer and Clark, 2017). The location of these cells within the TM dictates their properties. TM cells in the uveal and corneoscleral portions act as endothelial cells. The endothelial-like TMC are involved in mediating inflammation. These cells can secret various enzymes and cytokines, such as Interleukin 8 (IL-8 or chemokine (C-X-C motif) ligand 8, CXCL8), Interleukin 6 (IL-6), and Monocyte Chemoattractant Protein-1 (MCP1 or chemokine (C-C motif) ligand 2, CCL2) in response to stimuli, including mechanical stretch, laser irradiation and proinflammatory cytokines. These factors can also be secreted in the absence of stimuli and can modulate TM and ECM functions (Shifera et al., 2010). Moreover, similar to macrophages, TMC have the property to clear cell debris in order to prevent it from entering the iridocorneal angle. The TMC in the juxtacanalicular region exhibit an elongated morphology and function similar to both fibroblasts and smooth muscle cells. They secrete ECM proteins such as fibronectin, collagens, elastin, fibrillin, and proteoglycans, as well as degradative enzymes like matrix metalloproteinases (MMPs) (Buffault et al., 2020).

The MMP-mediated turnover of ECM reduces the outflow resistance of the conventional outflow pathway while helping maintain IOP stability. Studies indicate that when IOP increases, tissue inhibitors of metalloproteinase-2 (TIMP-2) decrease and MMP-2 expression increases (Bradley et al., 2001). Based on these results, TM cells respond to IOP increase by stretching or distortion the ECM and, in turn, increasing MMP expression and decreasing TIMP expression provide intraocular pressure homeostasis. Fibronectin is one of the major ECM proteins in the TM, has an important function in regulating IOP. In patients with primary open angle glaucoma (POAG) and elderly people increased expression of fibronectin has been observed in the TM and Schlemm's canal. This augmented fibronectin level in POAG may be attributed to elevated transforming growth factor-β2 (TGF-β2) levels. Evidence indicates that TGF-β2 elevates fibronectin levels in the TM both *in vivo* and *in vitro* (Faralli et al., 2019b; Fleenor et al., 2006). Fibronectin impacts IOP by increasing ECM stiffness and regulating the deposition of collagen IV,

laminin and fibrillin. Integrins also play an important role in raising IOP, with more than 10 different integrins identified to be associated with the TM in the outflow pathway. Integrin αvβ3 is an important integrin that regulates TGF-β1 activity and vascular endothelial growth factor (VEGF) receptor-2 expression. Furthermore, αvβ3-integrin affects TGF-β2 and influences IOP (Filla et al., 2021). The effects of other enzymes or cytokines on IOP are displayed in table 1.

Enzymes/Cytokines	**Effect on IOP**	**Reference**
Interleukin-1 beta (IL-1β)	Increase IOP	(Wooff et al., 2019)
Interleukin-6 (IL-6)	Increase IOP	(Ulhaq et al., 2020)
Interleukin-8 (IL-8)	Increase IOP	(Chono et al., 2018)
Matrix metalloproteinases (MMPs)	Decrease IOP	(Kim and Lim, 2022)
Monocyte Chemoattractant Protein-1 (MCP1 or CCL2)	Increase IOP	(Lee et al., 2021)
Rho kinase (ROCK)	Increase IOP	(Honjo and Tanihara, 2018)
Transforming growth factor-beta (TGFβ)	Increase IOP	(Hill et al., 2018)
Tumor necrosis factor-alpha (TNF-α)	Increase IOP	(Kondkar et al., 2018)
Vascular endothelial growth factor (VEGF)	Decrease IOP	(Kampougeris et al., 2013)

Table 1. Key enzymes and cytokines and their effect on IOP.

During the culture of human trabecular meshwork (HTM) cells, contaminations from neighboring cells, such as ciliary muscle cells, scleral spur cells, sclera fibroblasts, corneal endothelia, keratocytes, and Schlemm's canal endothelia may occur (Stamer and Clark, 2017). Additional identification methods are necessary because morphology alone

is inadequate for the identification of TM cells. Myocilin expression is higher in HTM cells compared to neighboring cells, but its expression decreases during the cell culturing process (Stamer and Clark, 2017). However, treatment with glucocorticoids dramatically upregulates myocillin expression in HTM cells, but not in neighboring cells (Stamer and Clark, 2017). Therefore, glucocoticoids-induced myocilin expression is the most reliable way to identify HTM cells. In addition, glucocorticoid treatment results in an upregulation of alpha - smooth muscle actin (α-SMA), and fibronectin expression in HTM cells (Steely et al., 1992; Yemanyi et al., 2020).

1.4 Glaucoma

Glaucoma is a group of eye diseases, also referred to as optic neuropathies. In 2020, over 76 million individuals worldwide suffer from this disease , with projections indicating the number will reach approximately 111.8 million by 2040 (Allison et al., 2020). However, glaucoma can remain asymptomatic until the disease reaches an advanced stage. The prevalence of undiagnosed and untreated glaucoma poses a heightened risk of vision loss, particularly in Africa and Asia (Soh et al., 2021). Glaucoma can be classified into two categories: open-angle glaucoma (OAG) and angle-closure glaucoma (ACG). This classification is based on the angle formation by the outflow pathway from the anterior chamber of the eye and the location where aqueous humor is blocked from exiting the eye (Stein et al., 2021). Glaucoma can be categorized into primary and secondary types based on the underlying cause including pigment glaucoma, traumatic glaucoma, neovascular glaucoma, uveitic glaucoma among others (Stein et al., 2021). Progressive degeneration of retinal ganglion cells (RGCs) is a hallmark of glaucomatous damage. This damage is believed to be associated with the optic nerve head or optic disc, the structure through which the nerve fibers passes is the lamina cribrosa (LC). The fenestrated LC region undergoes backward bowing in glaucoma, exerting pressure on and compressing the nerve fibers, ultimately resulting in vision loss (Quigley, 1999). While the pathophysiology of glaucoma remains incompletely understood, several theories exist.

The biomechanical theory states that elevated IOP is a major and variable risk factor for glaucoma, causing mechanical stress and tension on the eye. In addition, cerebrospinal fluid pressure (CSFP) within the subarachnoid space and blood pressure (BP) within the central retinal vessels can impact the biomechanical condition of the optic nerve hypoplasia (ONH) (Hua et al., 2018). A second theory suggests that insufficient blood supply to the ONH is also a factor. The current understanding is that high IOP leads to inadequate blood supply to the ONH. However, there are some glaucoma patients with normal IOP, known as normal-tension glaucoma (NTG). Some studies have reported a reduction in ocular reperfusion among glaucoma patients compared to healthy individuals, which is due to vascular dysregulation. Unstable ocular blood flow (OBF) may result in unstable ocular perfusion, leading to ischemia and reperfusion damage to the retina and ONH (Hua et al., 2018). Another theory suggests that inflammation may play a role in the development of glaucoma. Glial cells in the retina or neuronal tissue and TM cells in the TM regulate the inflammatory responses of the eye. Inflammation is a complex biological response that occurs in response to various stimuli, including oxidative stress, injury, and infection. According to the inflammation theory, glaucomatous damage to the optic nerve is not solely caused by elevated IOP, but rather a combination of elevated IOP and ongoing low-grade inflammation within the eye. Studies have indicated that glaucoma patients exhibit increased levels of pro-inflammatory cytokines and other inflammation markers in the AH and TM (Freedman and Iserovich, 2013; Taurone et al., 2015). These findings imply that inflammation may contribute to TM dysfunction and the development of elevated IOP. In general, para-inflammation is characterized as a cellular response to noxious stress or dysfunction and is an intermediate stage between normal or basal and inflammatory states. Stress or dysfunction in tissues can lead to detrimental consequences. However, a physiological level of para-inflammation is essential for maintaining tissue homeostasis and restoring functionality (Baudouin et al., 2021). Para-inflammation is dysregulated in glaucoma, which is necessary for protection of homeostasis in the RGCs, ONH and TM cells. Dysregulation of the inflammatory balance

in the eye may cause chronic inflammation, leading to loss of TM cells and RGCs or degeneration of the ONH (Baudouin et al., 2021).

Glaucoma treatment varies based on the specific type of glaucoma. Unique treatment modalities are required for each type. However, effective control of IOP is imperative in preventing glaucoma. The use of topical medications is generally the first line of treatment in reducing and regulating IOP. Various medications such as prostaglandin analogs, beta blockers, alpha 2-adrenergic agonists, and carbonic anhydrase inhibitors lower IOP in different ways and to varying degrees (Li et al., 2016). However, systemic and local side effects like liver or kidney disease, conjunctival hyperemia, and dry eye may occur (Schuster et al., 2020). Laser therapy may be utilized if topical medication fails to lower the IOP or achieve the target pressure. Laser was first used in the 1970s to lower IOP. Laser trabeculoplasty is a kind of therapy with multiple spots of thermal laser applied directly to the TM to alter the structure and to increase the aqueous humor outflow. To date, it has increasingly become a complementary method to lower IOP. However, there are potential complications inflammation, pupillary deformity and excessively low IOP, etc. (Schuster et al., 2020). Surgical intervention should be considered when non-surgical treatments fail to effectively lower IOP or lead to complications. In recent years, the available surgical options for treating ocular conditions have expanded, including minimally invasive, filtering, and nonfiltering types of surgery. Among these procedures, trabeculectomy is considered a standard approach that involves creating an additional drainage pathway under the conjunctiva, forming a "bleb". However, in certain cases, fibroblasts from the Tenons layer or the conjunctiva may obstruct this supplementary outflow pathway. Risk factors for surgical failure due to scarring include previous surgeries with conjunctival scars, extended use of topical medication, conjunctival and intraocular inflammation and young age (Schlunck et al., 2016).

1.5 The role of Thrombospondin-1 (TSP-1) in the development of glaucoma and trabeculectomy failure

Recent studies have shown that TSP-1 is related to intraocular pressure and glaucoma (Haddadin et al., 2012). It has also been associated with failure of previous trabeculectomy (Zhu et al., 2019). During the progression of glaucoma in animal models, a substantial increase in TSP-1 levels was found in AH. In addition, elevated levels of TSP-1 have been detected in the post-operative conjunctival "bleb". In non-ophthalmic studies, TSP-1 has been shown to play a role in wound healing and to contribute to tissue fibrosis (Moretti et al., 2022).

Additionally, a recent study has indicated that TSP-1 may display minor genetic variations in a highly preserved segment of the TSP-1 molecule. Nonetheless, these slight modifications in TSP-1 result in a congenital type of glaucoma, accumulation of ECM, and later dysfunction of the TM (Fu et al., 2022). Genetically modified mice with a $Thbs^{R1034C}$ mutation in the TSP-1 gene exhibit elevated intraocular pressure, reduced outflow rate from the anterior chamber, and loss of retinal ganglion cells. Juxtacanalicular trabecular meshwork, which is responsible for aqueous humor outflow, displays abnormal extracellular matrix accumulation and morphology in the histological analysis. It appears that a single genetic modification of TSP-1 leads to protein misfolding, causing accumulation in the anterior chamber of the eye, which is later joined by fibronectin accumulation which can also bind TSP-1 (Fu et al., 2022).

1.6 Gene sequencing reveal elevated TSP-1 levels in patients with glaucoma

To evaluate the possibility of an *in vitro* study, various Gene Expression Omnibus (GEO, public date repository) databases (GSE123100 and GSE 148371) of glaucoma tissues were analyzed for the expression of TSP-1 (the method of this database analysis is described in methods). Here TSP-1 mRNA was discovered to be up-regulated in HTM tissues from glaucoma patients. The level of up-regulation was higher in glaucoma patients (p value < 0.01) compared to normal donors, with a log2 fold change of 4.7239.

A depiction of TSP-1 gene expression in glaucoma patients (1 patient with POAG and 4 with and normal subjects is shown in figure 2). With the assistance of the String program (https://string-db.org/), information regarding the proteins that are involved in the TSP-1 signal processing was revealed. The top 10 proteins involved in signal processing are fibronectin 1 (FN1), cluster of differentiation 47 (CD47), cluster of differentiation 36 (CD36), lysosome membrane protein 2 (SCARB2), matrix metalloproteinase-9 (MMP-9), scavenger receptor class B member 1 (SCARB1), syndecan 1 (SDC1), integrin beta-1 (ITGB1), Calreticulin (CALR), and matrix metalloproteinase-2 (MMP-2), as depicted in figure 3 and table 2. The gene expression of CD47, however, did not exhibit a significant increase. CD36, calreticulin (CALR), syndecan 4 (SDC4), integrin subunit beta 3 (ITGB3) and neuroligin 1 (NLGN1) exhibited no significant alterations. The changes of other genes are depicted in table 2.

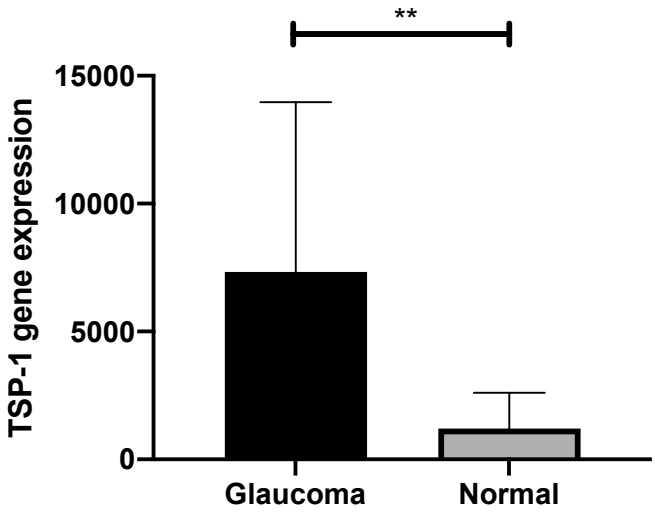

Figure 2. TSP-1 gene expression in the HTM tissue of glaucoma patients.
The black bar shows the TSP-1 expression of the glaucoma group (n = 7), while the gray bar shows the TSP-1 gene expression of the normal group (n = 8). The TSP-1 gene level is higher in glaucoma HTM tissues. **p value <0.01 (Mann-Whitney test). The analysis utilized publicly available datasets from the GEO database (GSE123100 and GSE 148371).

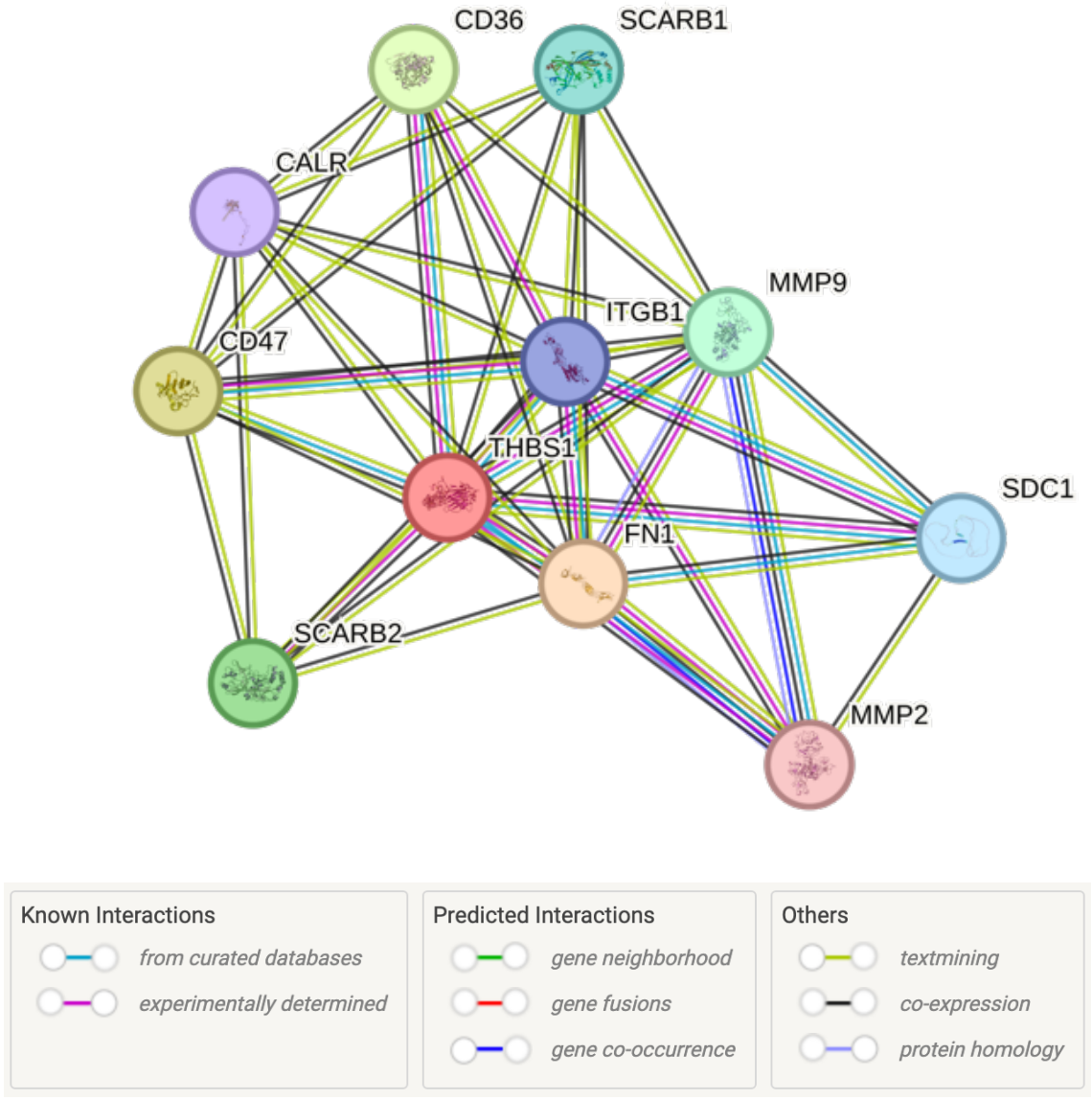

Figure 3. The potential interactions of TSP-1 (also known as THBS1).
The top 10 proteins that associate with TSP-1 via String program. CD47 is included. The inset in the bottom of diagram suggests different associations by which these proteins may be related.

Gene name	Protein name	Log2 fold change	Effect on glaucoma
TSP-1 (THBS1)	Thrombospondin-1	4.7239***	IOP regulation (Haddadin et al., 2012)
CD47	Leukocyte surface antigen CD47	-0.4572	Protected against cone degeneration(Wang et al., 2021)
CD36	Platelet glycoprotein 4	1.7420[#]	Mediated RGCs injury (Yang et al., 2022)
FN1	Fibronectin 1	4.3819***	Increased IOP (Faralli et al., 2019b)
MMP9	Matrix metalloproteinase-9	-2.1898	TM abnormal IOP control and loss of RGCs (Kim and Lim, 2022)
SCARB2	Lysosome membrane protein 2	1.9914**	Unknown
SCARB1	Scavenger receptor class B member 1	0.0342	Unknown
SDC1	Syndecan-1	3.5943***	Unknown
ITGB1	Integrin beta-1	0.1995	Unknown
CALR	Calreticulin	0.2210	Unknown
MMP2	Matrix metalloproteinase-2	0.9616	TM abnormal IOP control (Kim and Lim, 2022)

Table 2. Comparison of Differential Gene Expression in Trabecular Meshwork Tissues of Glaucomatous and Normal Eyes.

*** adjusted p value < 0.0001. ** adjusted p value < 0.01. [#] p value < 0.05 but adjusted p value >0.05. IOP, intraocular pressure. RGCs, retina ganglion cells. TM, trabecular meshwork.

1.7 TSP-1

TSP-1 belongs to the family of matricellular proteins, of which five calcium-binding glycoproteins with oligomeric and multidomain have been discovered to date (TSP-1, TSP-2, TSP-3, TSP-4 and TSP-5) (Adams and Lawler, 2011). Mammalian TSPs have numerous physiological and pathophysiological functions, including impacts on angiogenesis, inflammation, wound healing and tumorigenesis (Adams and Lawler, 2011). These processes are mechanistically mediated by interactions with the cells surface and various ligands, such as integrins, growth factors, cytokines, proteases, and ECM components (Adams and Lawler, 2011).

TSP-1 is a glycoprotein that is multimodular and belongs to the matricellular proteins found in the ECM. It was first isolated from platelets after they were treated with thrombin (Lawler et al., 1978). TSP-1 consists of a complex multidomain structure (figure 4). By interacting with various molecules, each of these domains control specific cellular functions. TSP-1 contains an N-terminal globular domain. Heparin has been shown to be the major binding factor for the N-terminal domain (Elzie and Murphy-Ullrich, 2004). In addition, sulfatides, low-density lipoprotein receptor related protein (LRP), calreticulin (CRT), and integrins (α3β1, α4β1 and α6β1) (Elzie and Murphy-Ullrich, 2004) have been shown to interact with it. The type I domain comprises thrombospondin structural homology repeats (TSRs) with three repetitions, which activate cluster of differentiation 36 (CD36) and induce apoptosis in endothelial cells (Yang et al., 2022). CD36 contains the carboxy-terminal intracellular domain (COOH-terminal), the amino-terminal intracellular domain (NH2-terminal), an extracellular domain, and two transmembrane domains (Yang et al., 2022). TSP-1 is a protein-associated ligand that can bind to CD36 (figure 4) (Yang et al., 2022). In addition, type I repeats can interact with matrix metallopeptidase (MMP)-2, MMP-9, and latent TGF-β. This is followed type II repeats, which have been found to interact with three epidermal growth factor-like (EGF) domains. Type II repeats have been shown to interact with EGF receptor and β1 integrins (Adams and Lawler, 2011). While TSP-1 also contains seven type III repeats and has been shown

to bind to fibroblast growth factor 2 (FGF2), calcium, integrin αIIβ3, and integrin αVβ3 (Adams and Lawler, 2011). In addition, TSP-1 binds to CD47 through its COOH-terminal domain and is known to be an integrin-associated protein (Adams and Lawler, 2011).

TSP-1 is expressed in various cell types, such as endothelial cells, epithelial cells, fibroblasts, adipocytes, vascular smooth muscle cells, monocytes, and macrophages (Kale et al., 2021). Additionally, TSP-1 is also expressed in various regions of the eye, including the cornea, lens, RPE, and trabecular meshwork, among others (Adams and Lawler, 2011; Flügel-Koch et al., 2004).

TSP-1 interacts independently with latent TGF-β, which is a crucial player in glaucoma pathology. In the context of increased IOP in glaucoma, cyclic mechanical stress induces TGF-β1 in the TM and LC, and it also induces TSP-1 in LC cells (Flügel-Koch et al., 2004). There is a possibility that the expression of TSP-1 in the adult TM may be related to its adhesive properties, because remodeling of the contacts between tissue cells and the matrix in the juxtacanalicular region seems to be an important factor in modulating outflow resistance in the TM (Flügel-Koch et al., 2004). Elevated expression of TSP-1 and TGF-β was observed in the TM cells of glaucoma patients compared to normal patients (Flügel-Koch et al., 2004). TSP-1 and TGF-β2 levels in the aqueous humor are higher in primary angle-closure glaucoma (PACG) eyes with failed trabeculectomy than in those with successful trabeculectomy after one year (Zhu et al., 2019).

1.8 CD47

CD47 is a transmembrane receptor that is widely expressed and is also known as integrin-associated protein (IAP) (Soto-Pantoja et al., 2013). CD47 has an extracellular N-terminal IgV domain, five transmembrane domains, and a short C-terminal intracellular tail. There are four alternatively spliced isoforms of CD47 that mainly differ in the length of their cytoplasmic tails (Soto-Pantoja et al., 2013). CD47 binds to macrophages via the ligand signal-regulatory protein alpha (SIRPα), acting as a "do not eat me" signal. Overexpression of CD47 occurs on the surface of numerous human tumor cells, which

allows such cells to escape immune system surveillance and elimination. Consequently, CD47 represents a potential target for the development of anti-tumor drug development. To this end, various clinical trials have been conducted utilizing an anti-CD47 antibody (Zhang et al., 2020).

CD47 is expressed in several cells of the eye, comprising HTM cells, ganglion cells, horizontal cells, bipolar cells, Müller cells, cones, rods (Sun et al., 2010). Additionally, CD47 could manipulate numerous biological functions of the aforementioned cells. Enhancing CD47-SIRPα signaling may offer a promising treatment approach for retinitis pigmentosa (RP) and other neurodegenerative disorders, according to a recent study (Wang et al., 2021). In the experimental autoimmune uveitis (EAU) model, it has recently found, that inflammation was reduced both locally in the eye and systemically in CD47-deficient mice (Okunuki et al., 2021).

In addition to SIRPα, CD47 acts as a receptor with a strong affinity for TSP-1. It binds via the N-terminal domain with the COOH-terminal domain of TSP-1 at picomolar concentrations (figure 4). TSP-1 binding to CD47, can regulate nitric oxide (NO). Its binding inhibits vascular NO signaling, leading to a reduction of blood flow, even when TSP-1 is present at very low concentrations (Isenberg et al., 2007). The binding of CD47 to TSP-1 inhibits autophosphorylation of VEGFR2, thereby preventing activation of endothelial nitric oxide synthase (eNOS). Additionally, CD47 impedes activation of eNOS by Ca2+/calmodulin, and activation of soluble guanylate cyclase (sGC) by NO and downstream cyclic guanosine 3', 5'-monophosphate (cGMP)-dependent protein kinase by cGMP (Yao et al., 2011).

Ischemia-reperfusion injury (IRI) is the tissue damage that occurs when blood flow is restored after ischemia or oxygen deprivation. It plays an important role in myocardial infarction, stroke, and organ transplant failure. Multiple studies have demonstrated upregulation of TSP-1 and CD47 during IRI. Furthermore, blocking or genetic deletion of CD47 has shown to prevent IRI in soft tissue, liver, and kidney (Rogers et al., 2012). Furthermore, TSP-1-CD47 is correlated with age-related illnesses, including

cardiovascular disease, cancer, and type-2 diabetes among others. In the process of aging, TSP-1 and CD47 levels rise exclusively in the vascular systems of both humans and mice, causing disruption to crucial cellular functions such as blood circulation, angiogenesis, cellular rejuvenation, and glucose balance (Ghimire et al., 2020).

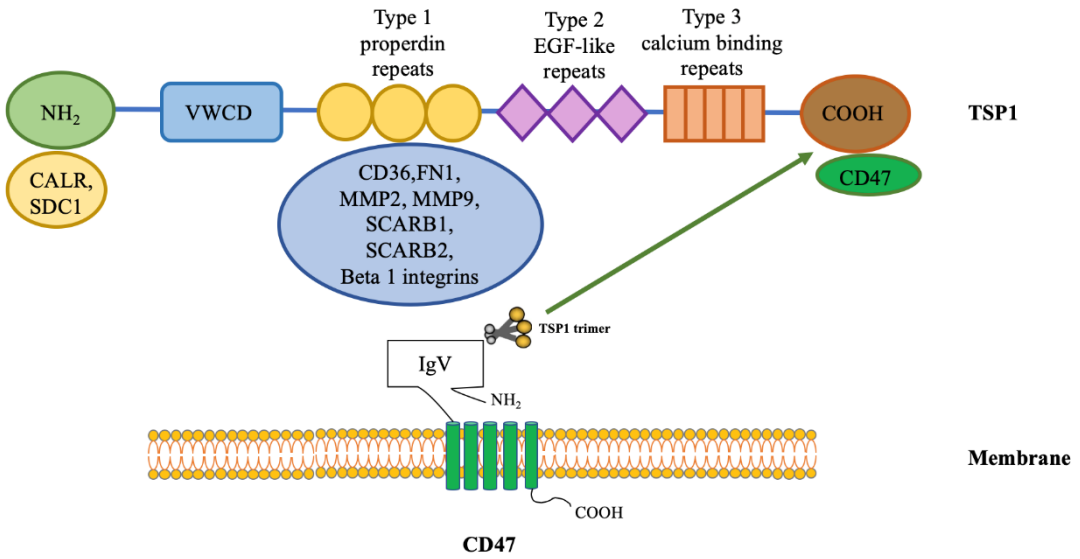

Figure 4. Model of TSP1 and its receptor CD47.
CD47 binds via N-terminal IgV domain with the COOH terminal domain of TSP-1. COOH, carboxylic acid. IgV, immunoglobulin variable. NH_2, amino-terminal intracellular domain. VWCD, the von Willebrand C domain.

1.9 The pressure chamber system

Elevated hydrostatic pressure (EHP) has been used to mimic ocular hypertension *in vitro* glaucoma models. Various studies have indicated that the EHP has an impact on cells located in the trabecular meshwork (Obazawa et al., 2004), Schlemm's canal (Burke et al., 2004), and retina (Böhm et al., 2016). Research focusing on elevated pressure *in vitro* provides a better understanding of the cellular mechanisms that could potentially play a role glaucoma development. This model is suitable for multiple cell cultures and even tissue cultures. Burke et.al conducted experiments using this model to investigate the effect of hydrostatic pressure (HP) and calcium chelators on human Schlemm's canal cells.

Their findings indicate that *in vivo*, calcium-sensitive junctions may play a role in outflow resistance (Burke et al., 2004).

One study used this pressure chamber system to cultivate retinal photoreceptor-derived cells and discovered that under EHP conditions, the high-mobility group box 1 protein (HMGB-1) might have a crucial role in continuous retinal cells damage under EHP condition (Böhm et al., 2016). In the present study, a previously described pressure chamber system was used for cultivating cell cultures under different HP conditions (Wang et al., 2020).

1.10 Aims of this study

High IOP is the most important and controllable risk factor of glaucoma. The structure of the TM also plays a critical role in the AH outflow facility. TSP-1/CD47 signaling may play a crucial role in regulating cell physiology and cytoprotection, particularly in redox control, inflammation, and self-renewal. In other cell systems, they have been shown to affect IRI. To investigate the role of CD47 and TSP-1 in glaucoma, HTM cells were exposed to varying pressures and tested with or without TSP-1 protein, the CD47 binding peptide of TSP-1 (P4N1), CD47 neutralizing antibody.

The primary aim of this study was to clarify the involvement of TSP-1/CD47 signaling in glaucoma and to determine whether anti-CD47 could offer a potential therapeutic strategy in glaucoma. In particular to:

(1) To determine the expression of CD47 and TSP-1 on HTM cells and to analyze the changes associated with HP and dexamethasone (Dex) stimulation.

(2) To investigate the impact of TSP-1 peptide and CD47 neutralizing antibody in HTM cells' viability and NO production.

(3) To investigate the effect of TSP-1 peptide and CD47 neutralizing antibody on the expression of ECM in HTM cells under different HP conditions and after Dex stimulation.

(4) To investigate the influence of TSP-1 peptide and CD47 neutralizing antibody on cytokines expression level associated with HP and Dex stimulation.

2 Materials and Methods

2.1 Materials

2.1.1 Chemicals

Name	Company
3- (4,5-Dimethylthiazol-2-yl)-2,5-diphenyltetrazolium bromide (MTT)	Carl Roth, Karlsruhe
Accutase	Sigma-Aldrich, Taufkirchen
Amphotericin B	VWR International, Darmstadt
Aqua bidest	Carl Roth, Karlsruhe
Dapi	Sigma-Aldrich, Taufkirchen
Demethylsulfoxid (DMSO)	Sigma-Aldrich, Taufkirchen
Ethanol ≥ 99.5%	Carl Roth, Karlsruhe
Ethylendiamintetraacetat (EDTA)	Sigma-Aldrich, Taufkirchen
Hydrochloric acid 6N standard solution (HCL)	Carl Roth, Karlsruhe
Methanol	Carl Roth, Karlsruhe
Mowiol	Sigma-Aldrich, Taufkirchen
N- (1-naphthyl) ethylenediamine	Sigma-Aldrich, Taufkirchen
N, N-dimethylformamide (DMF)	Sigma-Aldrich, Taufkirchen
Paraformaldehyde (PFA)	Sigma-Aldrich, Taufkirchen
Penicillin / Streptomycin (Pen/Strep)	PAA Laboratories, Pasching
Phosphate-buffered saline (PBS) powder	PAN-Biotech, Germany
Sodium chloride (NaCl)	Carl Roth, Karlsruhe
Sodium hydrogen carbonate (NaHCO3)	Carl Roth, Karlsruhe
Sodium hydroxide solution (NaOH)	Carl Roth, Karlsruhe
Sulfuric acid (H_2SO_4)	Carl Roth, Karlsruhe
TRIS-Base	Carl Roth, Karlsruhe
TRIS-HCl	Carl Roth, Karlsruhe
Triton X-100	Merck, Darmstadt

Trypan blue	Bio-Rad, Hercules, CA, USA
Tween 20	Carl Roth, Karlsruhe

2.1.2 Medium and serum

Name	Company
DMEM/Ham's F-12	Gibco, USA
Fetal Bovine Serum (FBS)	PAN-Biotech, Germany

2.1.3 Experimental consumables

Name	Company
Cell Counting Slides for TC20	Bio-Rad, Kauwenhoven, the Netherlands
Cell culture flask 25 cm^2	TPP, Trasadingen, Switzerland
Cell culture flask 75 cm^2 with filter screw caps	TPP, Trasadingen, Switzerland
Cell culture plates 6-,12-,24-,96-well, flat bottom	TPP, Trasadingen, Switzerland
Centrifuge tube 15ml,50ml	Biochrom, Berlin
Chamber Slide (Millicell) EZ Slide	Merck Millipore, Darmstadt
Cover slips	Carl Roth, Karlsruhe
Disposable latex gloves	Carl Roth, Karlsruhe
Eppendorf tubes 1.5ml, 2ml and 5ml	Carl Roth, Karlsruhe
Parafilm	Sigma-Aldrich, Taufkirchen
Petri dishes	Thermo Fisher, Dreieich
Pipette tips 10µl, 200µl, 1000µl	Sarstedt, Numbrecht
Serological pipettes 10ml	VWR International, Darmstadt
SuperFrost Plus Microscope Slides	Thermo Scientific, Schwerte
Terumo Syringe without Needle 1ml	Terumo, Eschborn
Test Tube, 12x75mm, blue	Beckman Coulter GmbH, Krefeld

2.1.4 Instruments

Name	Company
Apotome 2	Carl Zeiss, Jena
BluePower Power supply 500	SERVA Electrophoresis GmbH, Heidelberg
BlueFlash Semi-dry Blotter	SERVA Electrophoresis GmbH, Heidelberg
Easypet	Eppendorf Ag, Hamburg
Elisa Reader MRX-ELISA	Dynatech Laboratories, Sussex, UK
Eppendorf-Zentrifuge	Heraeus Holding, Hanau
Flow Cytometry CytoFLEX	Beckman Coulter GmbH, Krefeld
Fluorescence microscope Axio Imager M2	Carl Zeiss, Jena
Freezers -20°C	Liebherr-Baumaschinen, Dortmund
Freezers -80°C	Heraeus Holding, Hanau
Fridges 4°C	Heraeus Holding, Hanau
Gel Caster	Horfer, Inc. USA
Heating & drying ovens Memmert	Dunn laboratory technology, Asbach
Hera Cell Incubator	Heraeus Holding, Hanau
Heraeus Multifuge 3SR Plus	Heraeus Holding, Hanau
HERAsafe Safety Cabinets	Heraeus Holding, Hanau
Inverted microscope CK40	Olympus Germany, Hamburg
Magnetic stirrer hot plate	Heidolph Instrument, Kelheim
Microscope Olympus BX40 F4	Olympus Germany, Hamburg
Multipette M4	Eppendorf AG, Hamburg
NANOpure Diamond	Wilhelm Werner, Leverkusen
Olympus Binocular Microscope SZ-PT	Olympus Europe SE & Co. KG, Hamburg
Pipette, 10-, 200-, 1000 µl	Eppendorf AG, Hamburg

SERVA BlueShake 3D	SERVA Electrophoresis GmbH, Heidelberg
TC20 Automated Cell Counter	Bio-Rad, Kouwenhoven, Netherland
Thermomixer 5436	Eppendorf AG, Hamburg
Vacuum pump, KNF	Laboport, Village-Neuf, France
Vertical Protein Electrophoresis	Horfer, Inc. USA
Vortex mixer	Marienfeld, Mergentheim
Water bath	Haake Germany, Vreden

2.1.5 Reagents

2.1.5.1 Buffer and medium

Reagent	Component
DMEM/F12	12 g/L DMEM/Ham's F-12 Powder 2.438 g/L $NaHCO_3$, pH 7.2 Add 1 L A.dest.
PBS, 10 ×	9.55 g/L PBS powder dissolve in 5L A.dest.
TBS, 10 ×	24 g Tris Base powder 88 g NaCl Dissolved in 1 L A.dest., pH 7.6

2.1.5.2 Cell culture medium

Reagent	Component
Cell culture medium for HTM cells	DMEM/F12 10%FBS 1% Pen/strep 1% Amphotericin B

FBS	Heated in the water bath at 56℃ for 30 minutes to inactivate complements and stored at -20℃

2.1.5.3 Stimulation reagents

Reagent	Company
Anti-CD47 antibody	Invitrogen
Dexamethasone (Dex)	Sigma-Aldrich, Taufkirchen
Lipopolysaccharide (LPS) solution, 500×	Thermo Fisher (eBioscience), Dreieich
Thrombospondin-1, Human Platelet	Athens Research and Technology

Name	Sequence	Description	Company
P4N1	RFYVVMWK	CD47-binding fragment of TSP-1	EMC microcollections
P4G1	RFYGGMWK	Negative control of P4N1	EMC microcollections

2.1.5.4 Reagents for MTT test

Reagent	Component
MTT solution	Dissolve MTT in 1 × PBS (5mg/ml) Sterile filtered Storage protected from light at -20℃
Stop solution	50% A.dest 50% DMF 0.3M SDS Stored at RT

2.1.5.5 Reagents for Immunofluorescence (IF)

Reagent	Component
DAPI	Stock: 1mg/ml
	Usage: 1 µg/ml (1: 1000)
	Diluted in 1 × PBST
Fixation solution	4% paraformaldehyde in 1 × PBS
Goat serum	Sigma-Aldrich, Taufkirchen
Mowiol (mounting medium)	12 g Mowiol
	30 g glycerol
	30 ml A.dest.
	60 ml 0.2M TRIS-HCl buffer
Permeabilization buffer	0.1 Triton X-100 in A.dest.
Washing buffer	0.1% Tween-20 in 1 × PBS (PBST)

2.1.5.6 Reagents for immunohistochemical staining (IHC)

Reagent	Component
Acetate buffer (Solution A)	8.2 g sodium acetate
	dissolved in 1 L A.dest.
Acetate buffer (Solution B)	5.8 ml acetic acid (100%)
	refill to 1 L with A.dest.
Acetate buffer, pH 5	Mix 141 ml solution A with
	59 ml solution B
Substrate	20 mg 3-Amino-9-Ethylcarbazol
	dissolve in 5 ml DMF
	and 95 ml Acetate buffer
	filtrate solution and add 100 µl 37% H_2O_2

2.1.5.7 Reagents for flow cytometry

Reagent	Company
Cleaning solution Cytoflex "Flow Clean"	Beckman Coulter, Krefeld
Fixation and permeabilization concentrate and diluent	Thermo Fisher (eBioscience), Dreieich
Pass buffer Cytoflex "Sheath Fluid"	Beckman Coulter, Krefeld
Permeabilization buffer (10x)	Thermo Fisher (eBioscience), Dreieich
Washing buffer	1 × PBS pH 7.4

2.1.5.8 Reagents for Western-Blot

Reagent	Component/Company
4 × Protein Sample Loading Buffer	0.2M Tris-HCl 0.4M dithiothreitol (DTT) 277mM, 8.0% (w/v) SDS 6mM Bromophenol blue 4.3M Glycerol dissolved in A.dest.
Agarose solution	Agarose (0.5%)
Anode buffer I	18.17 g Tris-base 100 ml methanol 500 ml A.dest. PH 10.4, stored at RT for 4 weeks
Anode buffer II	1.52 g Tris-base 100 ml methanol 500 ml A.dest. PH 10.4, stored at RT for 4 weeks
APS, 10%	10% APS Dissolved in A.dest.

Blocking buffer	5% skim milk 5 g skim milk powder dissolved in 1 × TBST
Cathode buffer	1.52 g Tris-base 2.63 g ε-aminocaproic acid 100 ml methanol 500 ml A.dest. PH 9.4, stored at RT for 4 weeks
Electrophoresis Buffer, 5x	15.1 g Tris-base 94 g glycine 5 g SDS Dissolved in 1 L A.dest. Stored at room temperature (RT) for 4 weeks
Washing buffer	1 × TBS 0.1 % Tween-20

2.1.5.9 Reagents for NO-test

Reagent	Component
N- (1-Naphthyl) ethylene diamine solution	1% N-(1-naphthyl) ethylenediamine in absolute methanol
Sodium nitrite (NaNO2) standard	10mM
Sulfanilic acid solution	1% sulphanilic acid in 4N hydrochloric acid

2.1.5.10 Reagents for Arginase Assay

Reagent	Component/Company
Acid mixture (Stop solution)	H2SO4 (96%)

	H3PO4 (85%)
	H2O
	Proportion: 1:3:7
Alpha-isonitrosopropiophenone (ISPF)	Dissolved in 100% ethanol
L-arginine	0.5 M, PH 9.7
Leupeptin	Sigma-Aldrich, Taufkirchen
Lysis buffer	10 mM Tris-HCL, PH 7.4
	1 µM Pepstatin A
	1 µM Leupeptin
	0.4 % Triton X-100
Manganese II chloride ($MnCl_2$)	10 mM
Pepstatin A	Sigma-Aldrich, Taufkirchen
Standard urea solution	Dissolved in A.dest.
	Between 0.0625 µg/ml and 0.8µg/ml

2.1.6 Fluorochromes

Conjugate	**Full name**	**Laser line**	**Excitation/Emission (nm)**
AF488	Alexa Fluor 488	488	495/519
APC	Allophycocyanin	638	645/660
FITC	Fluorescein-5-isothiocyanate	488	493/525
FVD eFluor 780	Fix viability dye eFluor780	638	633/780
Strep/AF 594	Streptavidin / Alexa Fluor 594	488	590/617

2.1.7 Antibodies

2.1.7.1 Antibodies for IF

Name	Source/clone	Conjugate	Company
Anti-human CD47	Rabbit Polyclonal	Unconjugated	Abclonal
Anti-human myocilin	Rabbit Polyclonal	Unconjugated	SantaCruz
Anti-mouse/human fibronectin	Rabbit Polyclonal	Unconjugated	Invitrogen
Anti-mouse/human/rat collagen IV	Rabbit Polyclonal	Unconjugated	Invitrogen
Anti-mouse/human/rat smooth muscle actin (SMA)	Rabbit/17H19L35	Unconjugated	Invitrogen
Anti-thrombospondin1 (TSP-1)	Mouse/A6.1	Unconjugated	Invitrogen

2.1.7.2 Antibodies for IHC

Name	Source/clone	Conjugate	Company
Anti-thrombospondin1 (TSP-1)	Mouse/A6.1	Unconjugated	Invitrogen

2.1.7.3 Antibodies for flow cytometry

Name	Source/clone	Conjugate	Isotype	Company
Anti-human CD47	Mouse/2D3	APC	IgG1, κ	Invitrogen

2.1.7.4 Antibodies for Western blotting

Name	Source/clone	Company
Anti-human GAPDH	Mouse/mAb	Abclonal
Anti-human/mouse/rat CD47	Rabbit/pAb	Abclonal
Anti-human/mouse/rat THBS1	Rabbit/pAb	Abclonal
HRP Goat anti-mouse	Goat	Abclonal
HRP Goat anti-rabbit	Goat	Abclonal

2.1.8 Primary cells and cell lines

HTM cells used in this study were isolated from donor corneoscleral rims which were used for human cornea transplantation (document number: 2018-574-f-N, Ethikkommission der Ärztekammer Westfalen-Lippe und der Universität Münster). All experiments involving human tissues or cells were followed the tenets of the Declaration of Helsinki. Human Umbilical Vein Endothelial Cells (HUVEC) was from the American Type Culture Collection (ATCC, PCS-100-010™).

2.1.9 Software

Name	Company
Adobe Illustrator CC 23.0.1	Adobe Inc.
Adobe Photoshop CC 2019	Adobe Inc.
EndNote X9	Thomson ResearchSoft, Stamford, Connecticut, USA
GraphPad PRISM 8	GraphPad Software, La Jolla, California, USA
ImageJ 1.52a	National Institutes of Health, USA
Kaluza Analysis 2.1	Beckman Coulter, Indianapolis, USA
Microsoft Excel 2021	Microsoft, Redmond, Washington, USA
Microsoft PowerPoint 2021	Microsoft, Redmond, Washington, USA
Microsoft Word 2021	Microsoft, Redmond, Washington, USA
ZEN lite V2.3	Carl Zeiss, Jena, Thuringia, Germany

2.2 Methods

2.2.1 Experimental flow chart

Primary HTM cells were isolated from donor corneoscleral rims and cultured with complete cell culture medium (DMEM containing 10% FBS, 1% Pen-Strep and 1% Amphotericin B). HTM cells from passage 4 were used in all the experiments (figure 5).

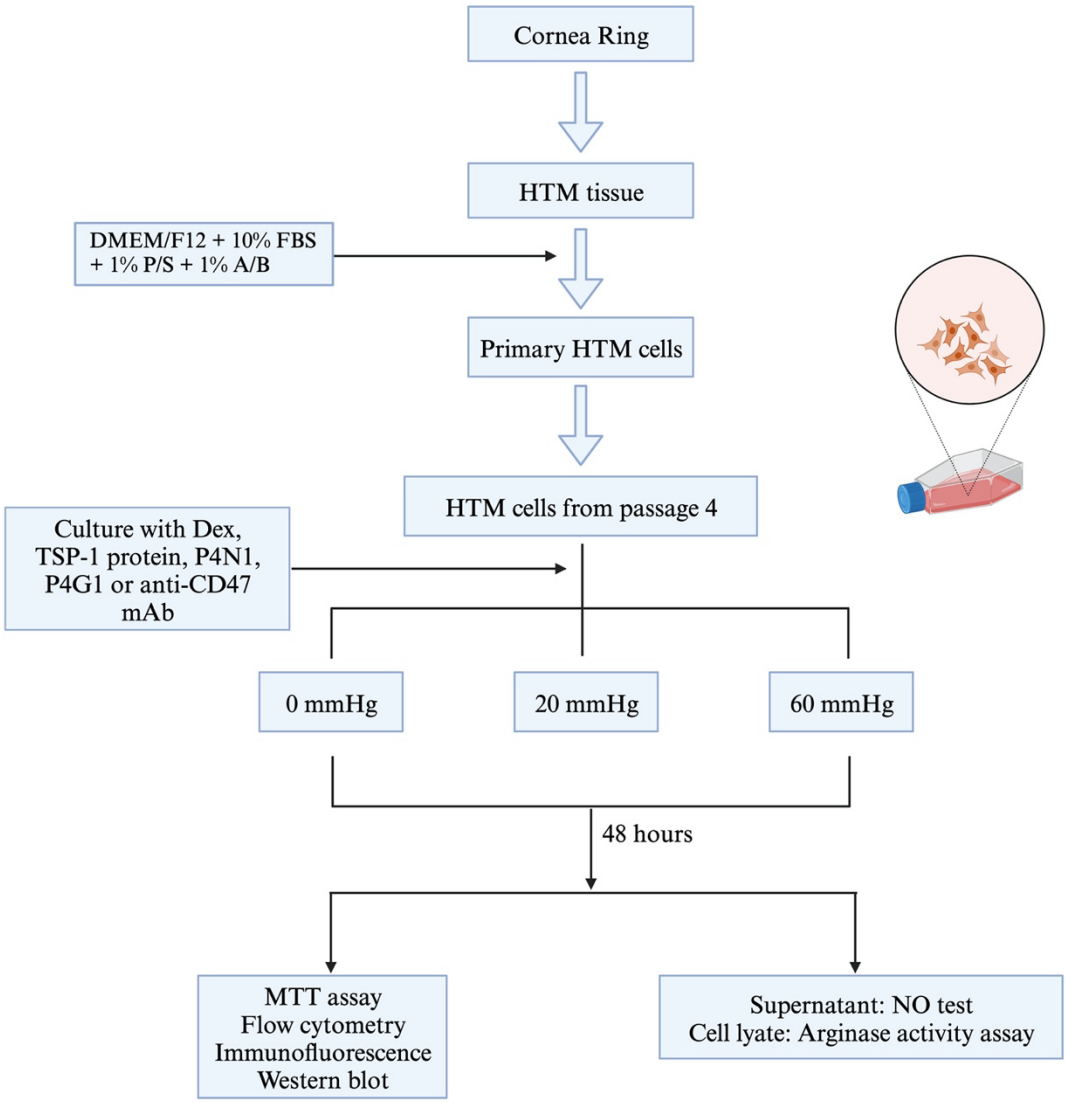

Figure 5. The experimental flow charts.
Primary cells were cultured with different treatments and HPs. After 48 hours, cells and / or cell culture supernatants were subjected to analysis via different immunological assays. CD47 = Cluster of Differentiation 47; Dex = dexamethasone; FBS = fetal bovine serum; HTM = human trabecular meshwork; NO = nitric oxide; TSP-1 = Thrombospondin 1. Created with BioRender.com.

2.2.2 Isolation and cultivation of HTM cells

HTM cells were isolated from corneoscleral rims acquired from human organ donors. Prior to use, all forceps and scissors were treated with 70% ethanol for 5 min to ensure sterility. The corneoscleral rims were then positioned in a sterile plastic Petri dish with the corneal endothelium side facing upward. Subsequently, iris and pigment were carefully removed using forceps. The TM tissue was then dissected from the tissue using sterile forceps under a binocular microscope. The TM tissue was then placed in a tissue culture dish and covered with sterile glass slides to ensure contact with the plastic bottom. Thirty mL of DMEM/F12 cell culture medium supplemented with 10% FCS, 1% Pen/Strep, and 1% amphotericin B were added. The plate was then incubated in a humidified incubator at 37°C and 5% CO_2 for 1 week. Once the primary cells had grown out of the tissue, the medium was replaced twice a week until the cells had grown into colonies and began coalescing. After removing the slide and TM tissue strips from the culture dish, the growing cells were cultured using HTM cell complete medium. The TM strips could then be transferred to a new plate and further cultured. The medium was replaced twice a week (every 3-5 days). Once the cells had reached 90% confluence, the medium was removed, and the adherent cells were washed twice with sterile 1 × PBS. To detach the TM cells from the plate, a 1 × Trypsin/EDTA solution was utilized, and the cells were then incubated at 37°C for 3 min. After adding 3ml of complete medium, the cells were detached by careful pipetting. The resulting cell suspension was collected in a sterile tube and centrifuged at 500 g for 5 min. The supernatant was discarded and the cells were resuspended with complete cell culture medium. The cell suspension was then distributed into cell culture flasks. The medium was replaced twice weekly, and cells were subcultured upon reaching 90% confluence. Cells from the fourth passage to sixth passages were utilized for all experiments.

2.2.3 Pressure chamber system

To mimic the influence of IOP in HTM, a pressure chamber system was utilized to provide the HP in this study. The system comprises of stainless steel cylindrical vessel with a diameter of 15 cm and a depth of 10 cm, furnished with a lid. It has one manometer, and an external connector to adjust the pressure. The intracameral pressure is constantly monitored by a manometer. The pressure can be set from 0 mmHg to 300 mmHg. For this study, pressures of 0 mmHg, 20 mmHg, or 60 mmHg were utilized. The chambers were incubated in a 37°C incubator with the lid open for 2 hours prior to cell incubation. During the initial day of incubation, the pressure was checked every 2 hours and followed by 3 times the next day.

2.2.4 Flow cytometry (Extracellular staining)

Culture medium of cells was discarded and cells were washed 3 times with sterile 1 × PBS. Cells were collected using Accutase solution and ice cold 1 × PBS/EDTA (20 mM) from the cell culture plates and transferred into a 50 ml round bottom polypropylene tube. The cells were then centrifuged at 500 g for 10 min, the supernatant was discarded and resuspended cells with 5 ml ice-cold 1 × PBS/EDTA. After calculated cell number, Fc Block (2 µl/10^6 cells) was then added and the cells were incubated at 4°C for 5 min. Washing 2 times with 1 × PBS/EDTA and centrifugation at 4°C at 500 g for 10 min. The cell concentration was adjusted to approximately 2 × 10^5 cells per staining and cells were divided equally into flow cytometry tubes (5 ml). The cells were then washed once with ice cold 1 × PBS/EDTA and centrifuged at 500 g for 10 min. Subsequently, 50 µl antibody solution was added (in 1 × PBS/EDTA) to each tube and incubated at 4°C for 45 min. Fixable Viability Dye (in 1 × PBS/EDTA, 1:2000) was added after incubation of 10 min. The cells were then washed using 600 µl 1 × PBS/EDTA and centrifuged at 500 g for 10 min. Cells were resuspended in 200 µl 1 × PBS/EDTA and transferred into blue PP tube for CytoFlex analysis and the obtained outcomes were analyzed utilizing the Kaluza software (figure 6).

100 µl of Ic Fix Buffer was then added to each tube and incubated for 20 min. The fixed cells were washed and incubated overnight at 4°C.

Laser	Filters	Dyes	Marker [Concentration mg/ml]	Amount (µl)	Isotype [Concentration, mg/ml]	Amount (µl)
488		FITC	CD47	2.5	Mouse IgG1	2.5
	780/60 LP	eFluor 780	Fixable viability Dye	1:2000	none	none

Table 3. Penal of extracellular staining for HTM cells in flow cytometry.
The penal of antibodies applied in extracellular staining in flow cytometry by CytoFlex analysis of HTM cells. HTM = human trabecular meshwork.

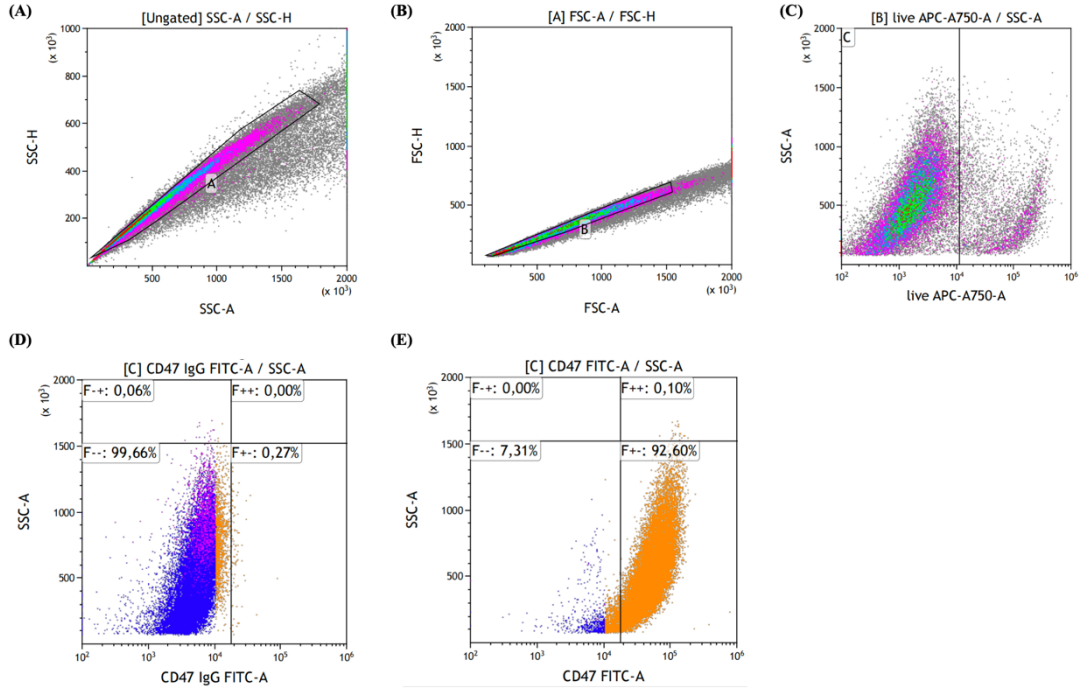

Figure 6. Representative gating strategy of Kaluza analysis.
(A) Ungated events from one HTM cells sample in the SSC-A/SSC-H window, gate A showed single cells. (B) Events gated from gate A were displayed in FSC-A/FSC-H, gate B showed single cells. (C) After gated by single cells (gate B), single live cell gate was set and positive events are depicted in the left area (gate C). (D) CD47 isotype control staining. (E) Extracellular staining of CD47 in HTM cells was analyzed. $CD47^{+}$ events were shown in the lower right area. The frequency of each population was calculated automatically by Kaluza software. HTM = human trabecular meshwork.

2.2.5 NO-test (Griess-reaction)

In this assay, nitrite ($NO2^{-}$) was measured to assess the concentration of NO in cell supernatants. The supernatants were collected after centrifuging of the cell culture medium. 50 µl sample or standard sample ($NaNO_2$, 1 mM, serially diluted 1:2 in cell culture medium) were added to the corresponding wells of a 96-well plate. Each sample was measured in triplicate. Then, 50 µl 1% sulfanilic acid solution (in 4 N HCl) and 10 µl concentrated HCl (37%) were added into each well and incubated for 10 min at RT in the dark. Subsequently, 50 µl of 1% N-(1-Naphathyl)-ethylenediamine solution (diluted in methanol) was added to each well. After 15 min, absorbance was measured at 550 nm. The NO concentration was then calculated using the standard curve.

2.2.6 Arginase activity assay

The arginase activity assay has been previously described (Corraliza, Campo et al. 1994). Cells were stimulated for 48 hours and exposed to elevated pressure, then harvested and counted. Subsequently, 200 µl of sample lyse buffer (10 mM Tris-HCL pH 7.4, 1 µM Pepstatin A, 1 µM Leupeptin and 0.4% Triton X-100) was used to lyse the cells. After 10 min, the cell lysates were centrifuged at 1800 rmp at 4°C for 10 min. The supernatants were collected for arginase assay.

40 µl of the sample lysates were mixed with 5 µl 10 mM $MnCl_2$ in a 1.5 mL tube. Subsequently, the mixture was heated at 56°C for 10 min to activate the enzyme. Then, 40 µl of 0.5 M L-arginine (pH 9.7) was added to each tube and incubated at 37°C for 1 hour. To stop the reaction, 400 µl of an acid mixture containing H_2SO_4 (96%), H_3PO_4 (85%) and H_2O (1:3:7) was added. After that, 25 µl α-isonitrosopropiophenone (ISPF), dissolved in 100% ethanol) was added to each tube and heated at 95°C for 30 min. A standard curve was plotted by increasing the urea concentration within the range of 0.0625 µg/ml and 0.8 µg/ml. 80 µl of the urea solution was added to a 1.5 ml tube with the appropriate concentration. Afterwards, 400 µl of acid mixture and 25 µl of ISPF were added and then heated at 95°C for 30 min. Subsequently, 200 µl of both the sample and

standard solutions were placed in a 96-well polystyrene plate to measure the absorbance at the wavelength of 550 nm (OD 550 nm). A linear regression analysis was conducted to determine the correlation between the OD 550 nm and urea concentration. For each reaction, one unit of enzyme activity was defined as the amount of enzyme that catalyzes the formation of 1 mmol of urea per minute. Each sample was measured a minimum of three times.

2.2.7 Cell migration and scratch assays

HTM cells were cultured in 24-well plates until they reached appropriate confluence levels (80%-90%). Following this step, a sterile pipette tip was utilized to create a straight-line scratch across the cell monolayer. The cells were then gently washed with 1 × PBS to remove any detached cells or debris. A fresh cell culture medium containing 1% serum and the antibodies was added. The plate was placed under a microscope and initial images of the scratch (time point 0 hour) were taken in order to document the initial gap. The plates were incubated at 37°C and 5% CO_2 to facilitate cell migration and closure of the scratch. At each time point of interest (0 hour, 6 hours, 12 hours and 24 hours), images of the scratch at specific time points were taken under the microscope. The ImageJ software were utilized to measure the percentage of the gap area.

2.2.8 MTT cell viability assay

HTM cells were harvested and cell suspension was centrifuged at 500 g for 5 min. The supernatant was discarded and cells were counted and adjusted to $1x10^5$ cells/ml in cell culture medium. 100 µl of cell suspension was added per well in 96-well plates and cultured for 24 hours. The outermost circle of the plate was filled with sterile 1 × PBS only (without cells). After the cells recovered and reattached, supernatant was removed carefully and 100 µl/well medium with different stimulations were added to the wells. Each stimulation was repeated six times per plate. Medium group was served as cell-based controls. The first column with cells added 1 M HCl at 30 min before add MTT

solution served as blank control. After different stimulations, remove the supernatant carefully and replaced by 100 µl 1 × PBS. 10 µl MTT reagent was added into each well and plates were incubated at 37°C for 4 hours. 100 µl of stop solution was added to each well and plates were incubated at 37°C in the dark overnight. The absorbance was read at 570 nm and cell viability was calculated as:

$$\text{Cell viability} = \frac{\text{ODsample} - \text{ODblank}}{\text{ODcontrol} - \text{ODblank}} \times 100\%$$

2.2.9 Immunofluorescence for HTM cells

HTM cells were harvested and adjusted to a concentration of $1x10^5$/ml using complete HTM cell culture medium (DMEM with 10% FBS, 1% Penicillin, and streptomycin solution). 400 µl of cell suspension was then added to each well of an eight-well chamber slide and cultured for 1 day. Subsequently, the culture medium was replaced with DMEM/F12 containing 1% FBS and 1% Pen/Strep. Cells were stimulated differently and incubated for 48 hours at different pressures (0, 20, or 60 mmHg).

The supernatant was discarded and the adherent cells were washed 3 times using sterile 1 × PBS. The cells were then fixed with 4% paraformaldehyde (PFA) for 10 min at RT and washed three times using ice cold 1 × PBS. Cells were then permeabilized with 0.1% Triton X-100 for 10 min at RT, followed by another 3 times washes. The cells were then blocked with 5% goat serum in PBST (1 × PBS with 0.1% tween) for 60 min at RT and washed 3 times with PBST. Cells were then incubated with primary antibodies (diluted in 1% goat serum in PBST) overnight at 4°C (table 4). Cells incubated without primary antibodies served as blank controls.

The next day, the cells were incubated at RT for 30 min to prevent detachment. They were then washed 3 times with 1 × PBS (containing 1% FBS) and incubated with secondary antibodies (diluted in PBST containing 1% FBS, 200 µl/well) for 30 min at RT in the dark. After washing three times, the cells were stained with DAPI, a nucleus stain, diluted in PBST with 1% FBS). After washing 3 times, the slides were covered with

fluorescence mounting medium and cover glass, taking care to avoid the formation of air bubbles. After air-drying, the slides were self-sealed in the dark at RT.

Primary antibody [stock concentration, mg/ml]	Dilution	Secondary antibody [stock concentration, mg/ml]	Dilution
CD47 [0.2]	1:100	Goat anti-rabbit AF488 [2]	1:1000
TSP1 [0.2]	1:100	Streptavidin AF594 [2]	1:1000
Fibronectin [0.2]	1:400	Goat anti-rabbit AF488 [2]	1:1000
α-SMA [0.2]	1:500	Goat anti-rabbit AF594 [2]	1:1000
Myocilin [0.2]	1:200	Goat anti-rabbit AF594 [2]	1:1000
Collagen IV [0.2]	1:200	Goat anti-mouse FITC [2]	1:500

Table 4. Dilutions of the antibodies used in immunofluorescence stainings for HTM cells.
Dilutions of the primary and corresponding secondary antibodies used in immunofluorescence stainings for HTM cells.

2.2.10 Immunohistochemical staining for HTM cells

HTM cells culture procedure was similar to immunofluorescence. After discarded the supernatant, adherent HTM cells were washed 3 times using 1 × PBS. The cells were then fixed with ice cold acetone for 20 min at RT and washed 3 times with 1 × PBS. The cells were then blocked with 5% FBS for 30 min at RT and discard the blocking buffer. Cells were then incubated with primary antibody (TSP-1, 1:100, diluted in 1% FBS in PBST) overnight at 4°C. Cells incubated with isotype control antibody served as negative control and without any antibody served as blank control.

The next day, the cells were incubated at RT for 30 min to prevent detachment. They were then washed 3 times with 1 × PBS (containing 1% FBS) and incubated with 3% hydrogen peroxide (H2O2) for 10 min. Incubated with streptavidin (1:1000, diluted in 1% FBS in PBST) at RT for 30 min then wash with 1 × PBS (containing 1% FBS). After washing 3 times, the cells were stained with substrate for 20 min and observe the reaction under microscope. Soaked the slides in acetate buffer (with 4% formalin) for 10 min then

rinse in 1% acetic acid for 15 seconds. Then Gill No.3 Hematoxilin solution was used, wash the slides with ddH2O when the cells turn to blue. After wash, the slides were covered with mounting medium and cover glass.

2.2.11 Biochemical techniques

Western blotting (WB) was utilized to identify protein expression in HTM cells.

2.2.11.1 Protein isolation

For protein isolation, HTM cells were stimulated in 6-well plates for 48 hours. Afterwards, the cell culture medium was removed, and the cells were washed 3 times with cold 1 × PBS. Adherent cells were then scraped off using a cold plastic scraper and the suspension was transferred to 1.5 ml pre-cooled microcentrifuge tubes. Centrifugation was done for 15 min at 12,000 g and 4°C). The supernatant was removed, and 100 µl of urea lysis buffer was subsequently added to the samples which were kept on ice for 30 min. Following that, the samples were centrifuged for 10 min at 12,000 g and 4°C), and the supernatants were then transferred into new tubes.

2.2.11.2 Bradford protein assay

The total protein concentration was measured using the Bradford protein assay, according to the manufacture's protocol (Bio-Rad). The dry concentration was diluted with ddH_2O (with 1 part dye reagent and 4 parts ddH_2O) and filtered to remove any excess particles. The solution can be stored at RT for up to 2 weeks.

The protein standard was prepared by dissolving 100 mg of BSA in 10 ml of ddH_2O. 10 µl of this solution were diluted in 990 µl of lysis buffer (1:100) to prepare a standard line with a concentration of 10 µg/µl. The protein assay has a linear range between 0.05 and 0.5 µg/µl. The concentration of the standard protein was also diluted within this range. The samples were diluted with ddH_2O at a ratio of 1:10. Afterwards, 10 µl of each sample dilution and the standard series were added in triplicate to a microtiter plate. 200 µl of the

diluted dye reagent was added to both the samples and standards. Subsequently, the microplate was incubated for 5 min at RT (not exceeding 1 hour). Following incubation, the absorbance was measured at 570 nm utilizing a plate photometer. The sample values were analyzed by referring to the BSA standard curve.

2.2.11.3 Sodium dodecyl sulfate polyacrylamide gel electrophoresis (SDS-PAGE)

The SDS-PAGE technique separates different proteins according to their chain length via sodium dodecyl sulfate (SDS), which has a strong affinity to proteins. Upon boiling with SDS, proteins receive a negative charge corresponding to their molecular size, allowing them to move in the acrylamide gel in proportion to their molecular size (Al-Tubuly, 2000).

To cast the gel, there were two steps: First, 8% or 10% resolving gel was prepared. The components are listed in the table 5. 10% APS and TEMED were added in the final step and mixed thoroughly. The resulting gel solution was then applied to the gel casting system, and absolute ethanol was added to the top of the gel to smooth the surface and prevent bubble formation. The resolving gel was allowed to stand at RT for approximately 30 min until the gel had hardened. The second step was the preparation of the 5% stacking gel, which was according to the recipe and poured over the resolving gel. A comb was inserted into the cast to form gel pockets for sample applications. The gel, once prepared, was either stored in a moist bag or used immediately.

For sample preparation, the isolated protein solution was dissolved in a 4 × Laemmli buffer and heated at 95°C and 12,000 g centrifuge for 3 min. To establish a size standard for comparative analysis of sample signals, 5 µl of a protein molecular weight marker were loaded into one of the gel pockets during gel loading. The gel loading process involved applying 20 – 30 µl of the respective samples to the remaining gel pockets. Following this, electrophoresis was initiated at 60 V, 80 mA, and 1 W for 30 minutes, after which the conditions were adjusted to 175 V, 120 mA, and 10 W. The progress of

gel electrophoresis was tracked by observing the migration of the bromophenolblue tracking dye.

	Stacking gel (5%)	Resolving gel (10%)	Resolving gel (8%)
H_2O	2.057 ml	4 ml	4.6 ml
30% Acrylamide	0.5 ml	3.3 ml	2.7 ml
1.5 M Tri/HCl PH 8.8	--	2.5 ml	2.5 ml
0.5 M Tris/HCl PH 6.8	380 µl	--	--
10% SDS	30 µl	10 µl	10 µl
10% APS	30 µl	10 µl	160 µl
TEMED	3 µl	4 µl	2 µl

Table 5. Recipe for SDS-PAGE Gel.

2.2.11.4 Western blotting

The WB technique was utilized to detect proteins that were separated via SDS-PAGE gel. The transferred proteins on the polyvinylidene difluoride (PVDF) membrane were detected by incubating them with a range of primary antibodies. The semi-dry blotting method was employed in this research (figure 7).

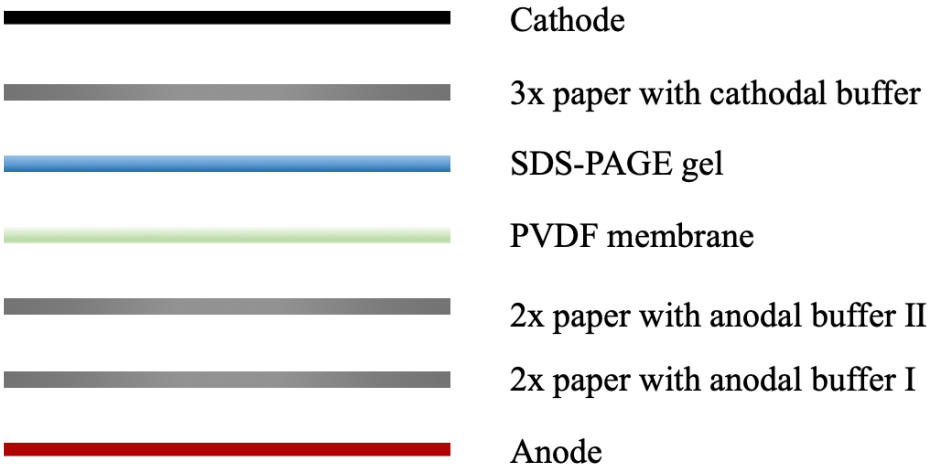

Figure 7. Semi-Dry-Blot.
Arrangement of the buffer-soaked filter papers, PVDF membrane and SDS-PAGE gel in a stack during the semi-dry blot process.

For each gel to be blotted, 7 stacks of blotting paper and a PVDF membrane were cut to the same size as the gel. Two stacks were soaked in anode buffer I, 2 stacks in anode buffer II and 3 stacks with cathodic buffer. The PVDF membrane was be incubated in 100% methanol for 2 min and then washed in ddH_2O before transferring. The stack was pressed from the centre to the edge with a roller. Electroblotting was carried out using the BlueFlash semi-dry blotter at 256 V and 50 W. The current was calculated by multiplying the area (in cm^2) of the PVDF membrane by the number of stacks and 2.5 mA: 2.5 mA × area (cm^2) × number of stacks. To prevent the instruments from being disrupted by gases produced, a 2 kg weighted bottle was utilized. The negative charged proteins migrated towards the anode during WB, which took 20 min using a 1 mm gel thickness and specified voltages.

In subsequent incubation steps, 5% skim milk dissolved in TBST (1 × TBS with 0.01% Tween-20) was used to block unspecific binding of proteins. The PVDF membrane was soaked in 5% skim milk and incubated under gentle agitation for 1 hour at RT. Specific primary antibodies were diluted in WB primary antibody diluent (Abclonal, Hubei, China). The membranes were incubated with primary antibodies at 4°C overnight. The following day, the membranes were washed 5 times with TBST for 5 min. Species-specific secondary antibodies were diluted in a solution of 2.5% skim milk and used to incubate blots at RT for 1 hour. Blots were washed 5 times for 5 min. The secondary antibodies were all linked to horseradish peroxidase, which generates a luminescent signal when cleaved by a luminescent agent. This signal can be captured by exposing photographic film. The membranes were covered with ECL solution and incubated for 3 min in a dark room. Excess liquid was drained from the membrane. The membrane was then wrapped in plastic foil and placed inside a film cassette, followed by exposure to blue X-ray films and development using a developer solution.

2.2.11.5 SDS-PAGE analysis with ImageJ

ImageJ is an open-source software used for quantification of protein bands on WB results. The relative amounts of proteins can be determined by calculating the ratio of each protein band to the loading control of the lane.

To analyze the results, the X-ray films were scanned and saved as tiff.files at 300 dots per inch (dpi). The density of protein bands was measured using ImageJ (1.52a) by opening and converting the image to an 8-bit format, applying background subtraction, and inverting the image to create a black background with grey band images. Each band was individual selected and measured. The integrated density (IntDen) was used for further analysis. The quantification process involved measuring the IntDen ratio between the target protein and housekeeping protein. The Intden ratio of the standard group was set to 1, against which the IntDen of the other groups was compared.

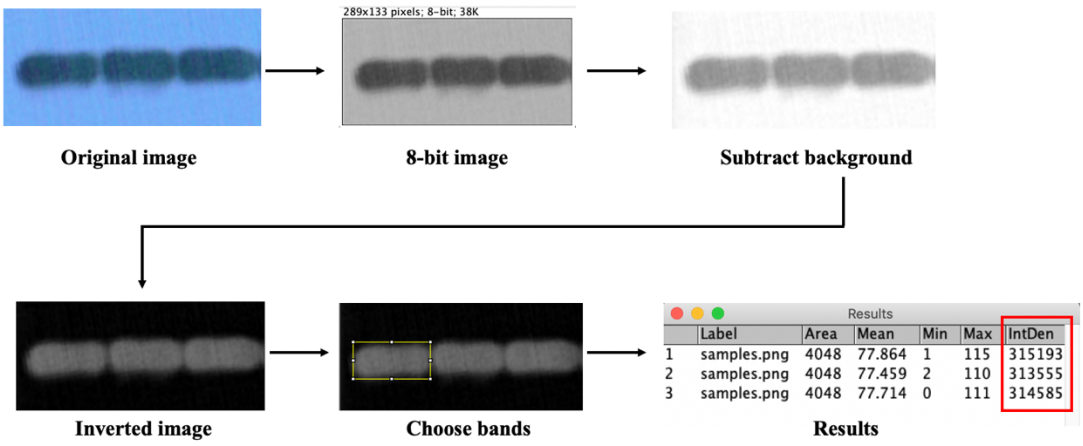

Figure 8. The integrated density of blots was measured by ImageJ software.

2.2.12 TSP-1 mRNA expression in glaucoma patients and normal HTM tissues

To determine the mRNA expression of TSP-1 in patients with glaucoma, a search was conducted in the Gene Expression Omnibus database (GEO, http://www.ncbi.nlm.nih.gov/geo) using the keywords "glaucoma and human trabecular meshwork" and selected the mRNA expression profiles from two datasets for this study. The first dataset, GSE123100, is based on the GPL20795 platform and included 7 glaucoma samples. One patient with primary open angle glaucoma (POAG) patient, 4

patients with acute angle closure glaucoma (AACG) and 3 patients with chronic angle closure glaucoma (CACG) patients were included in the first dataset. The second dataset, GSE148371, is based on GPL16791 platform and consists of 7 samples from 6 donors who have not reported any ocular disease. The two datasets were normalized using the "Limma" R package through the Sangerbox online analysis tool (http://vip.sangerbox.com/tool.html). The classical Bayesian algorithm was used to calculate the differentially-expressed genes (DEGs), with significance determined by the absolute value of log2 fold change > 1.5 and adjusted $p < 0.05$. To predict additional potential TSP-1 associated proteins, the online STRING program was utilized (https://string-db.org/).

2.2.13 Statistical analysis

Statistical analyses were performed using GraphPad Prism 8.0 (GraphPad, San Diego, CA, USA). Data are expressed as mean ± standard deviation of mean (SEM). An ANOVA (for normally distributed data) or the Kruskal-Wallis' test (for non-normally distributed data) was used to determine significant differences. $p < 0.05$ was considered statistically significant.

3 Results

3.1 Isolation and Morphology of HTM cells

HTM cells were isolated from donor corneoscleral rims available for cell isolation following corneal transplantation, as described in the materials and methods. The obtained tissues were cultured in DMEM/F12 medium in a 6-well plate. After 2 weeks of incubation, primary HTM cells began to migrate from the tissue (figure 9A). After 3 weeks of cultivation, the HTM cells were passaged. While there was variation in the shapes of the HTM cells, most exhibited a cobblestone-like pattern with overlapping processes. Healthy and normally cultured HTM cells are also contact inhibited and cells with low passage number with a doubling time of 2 to 7 days were used. The morphology of HTM cells remained unchanged following various stimulations and culture with different HP levels.

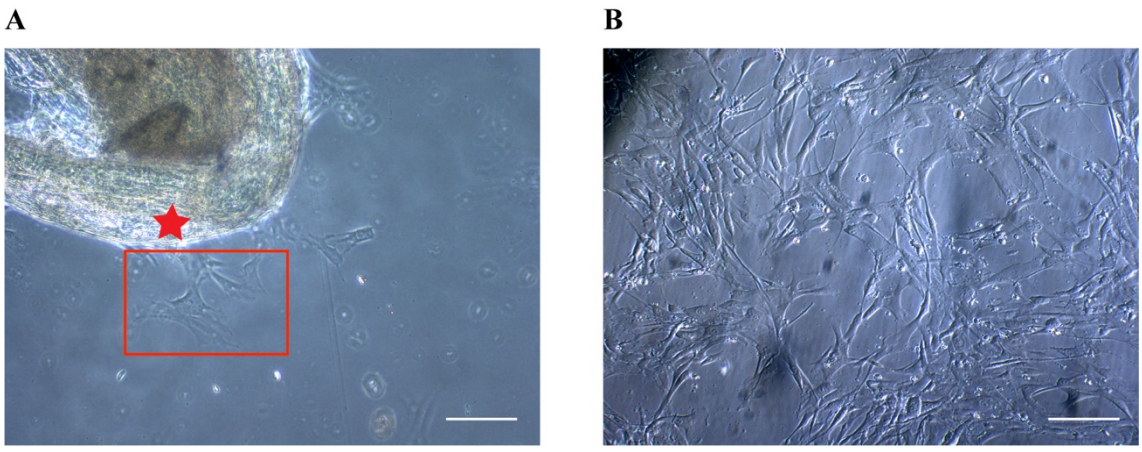

Figure 9. Morphology of HTM cells.
(A) HTM cells migrate out of the HTM tissue within 14 days. The red star highlights the original HTM tissue. The square indicates the HTM cells growing out of it. (B) The monolayer of HTM cells in passage 2. Scale bar = 25 µm.

3.2 Production of α-SMA, fibronectin and myocilin in isolated HTM cells following exposure to Dex

HTM cells were cultured with or without Dex (100 nM) for 48 hours, and subsequently stained with fibronectin, α-SMA or myocilin antibodies. The control group was stained

solely with the secondary antibody. Alpha-SMA was detected in the medium group and its staining was further elevated after induction by Dex. Immunostaining of fibronectin was observed in all HTM cells, however, staining was increased after incubation with Dex. Staining of myocilin was not detected in the medium group but was present after Dex treatment. In summary, the isolated HTM cells exhibited expression for the proteins α-SMA and fibronectin. Myocillin expression was observed solely following incubation with Dex (figure 10).

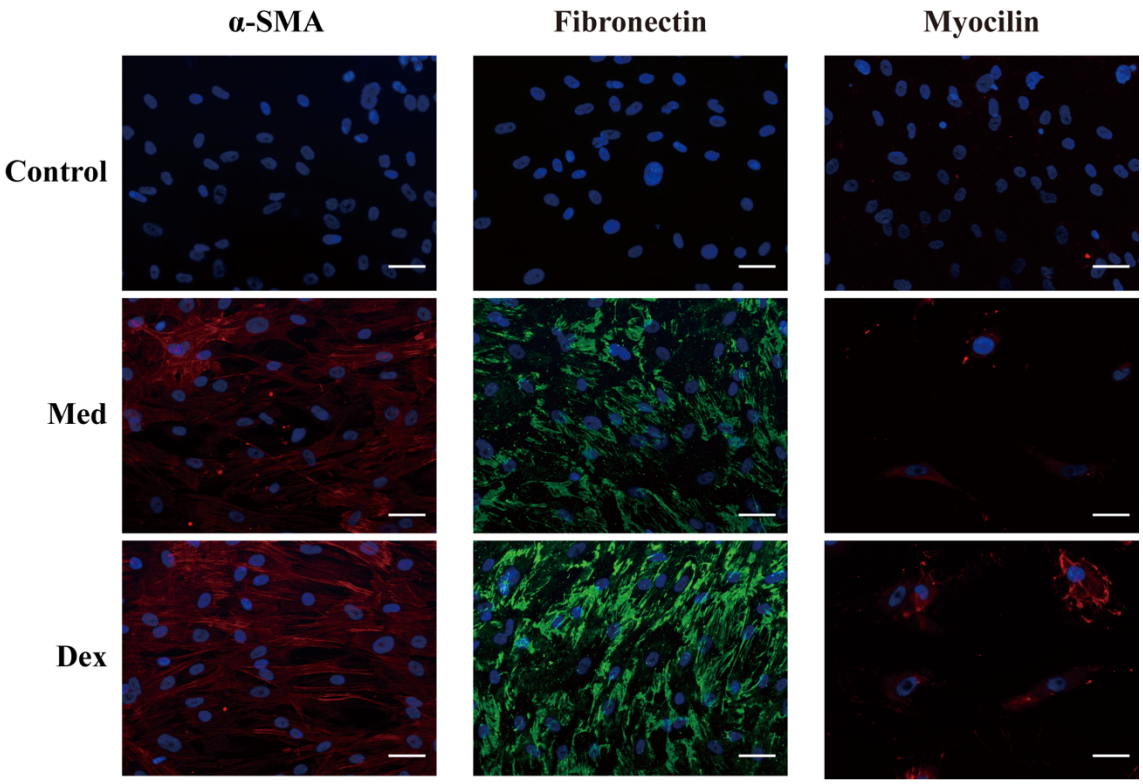

Figure 10. Alpha-SMA, fibronectin, and myocilin expression in cultivated HTM cells after exposure to Dex.
HTM cells were immunostained with antibodies targeting α-SMA (in AF594 channel, red), fibronectin (in AF488 channel, green) or myocilin (in AF594 channel, red). Control groups were only stained using the secondary antibodies. Nucleus were stained with DAPI. Merged images were shown. Scale bar = 50 µm. HTM = human trabecular meshwork. Med = medium group. Dex = dexamethasone group. α-SMA = Alpha smooth muscle actin.

3.3 Expression of TSP-1 in HTM cells

To assess the protein expression of TSP-1 in HTM cells, immunohistochemistry (IHC) and IF were performed. The blank control group was treated solely with the secondary antibody, while using isotype-matched nonspecific IgG antibody as negative control. In comparison to the blank control group and the isotype control group, the group treated with the primary antibody targeting TSP-1 exhibited clear brown color staining of HTM cells, as depicted in figure 11A. A similar staining pattern could also be found by IF staining which showed red color (figure 11B). In contrast, neither the blank control nor the isotype control showed positive staining, while nearly every cell exhibited positive staining in the group subjected with the monoclonal antibody targeting TSP-1, revealing the expression of TSP-1 in those cells.

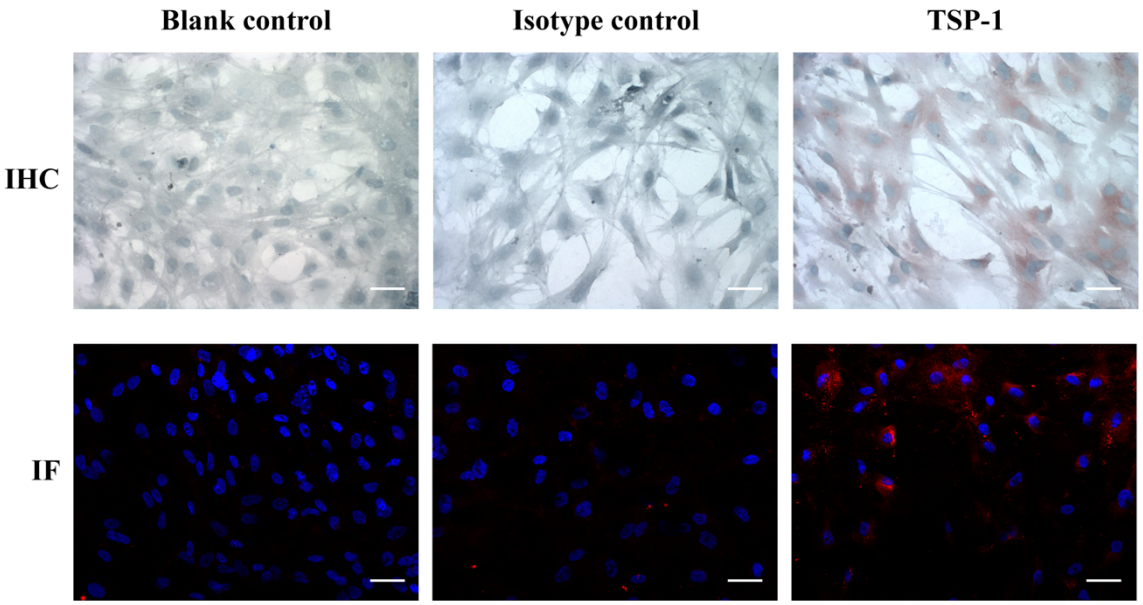

Figure 11. Expression of TSP-1 in isolated HTM cells.
Representative images of TSP-1 staining in HTM cells via IHC or IF. TSP-1 was stained in brown color in IHC. The Blank control and isotype control groups did not exhibit any brown color. In IF staining, TSP-1 (in AF594 channel, red) in HTM cells is visualized in the AF594 channel. Scale bar = 50 µm. HTM = human trabecular meshwork. TSP-1 = thrombospondin-1. IHC = immunohistochemistry. IF = immunofluorescence.

3.4 Expression of CD47 in cultivated HTM cells

To assess CD47 expression on HTM cells, flow cytometry and IF were performed. As depicted in figure 12A, the analysis of HTM cells using flow cytometry showed that 92.69% of these cells were positively stained for CD47, which indicates expression of the CD47 protein. In the IF staining, specific staining for CD47 was clearly observed in most of the HTM cells compared to the control group without primary antibody targeting CD47 (figure 12B).

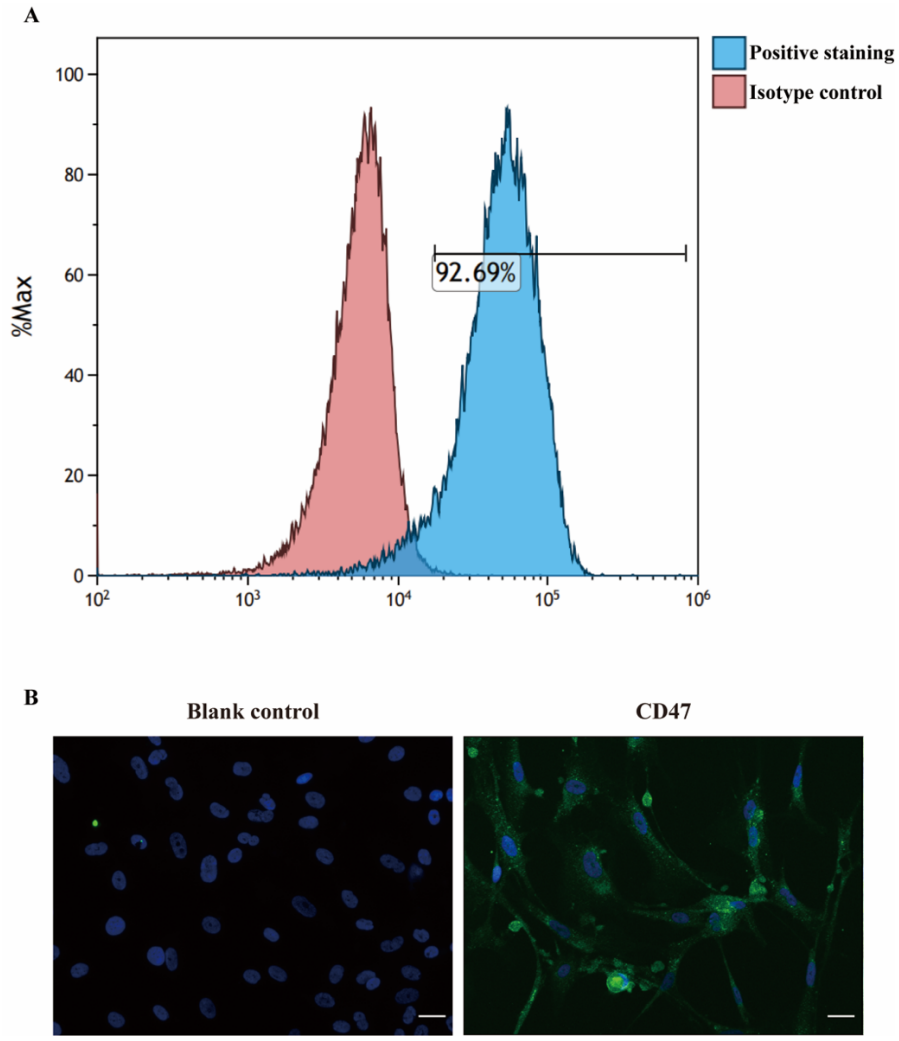

Figure 12. Expression of CD47 on isolated HTM cells after cell culture.
(A) Flow cytometry of CD47 on HTM cells. The blue graph depicts the positive staining for CD47, while the red color shows the isotype control. (B) Immunofluorescence of CD47 on HTM cells. Left: Blank control (secondary antibody control), right: CD47 staining in HTM cells (AF488 channel, green). Scale bar = 50 µm. HTM = human trabecular meshwork. CD47 = cluster of differentiation 47.

3.5 TSP-1 expression in HTM cells after exposure to Dex in combination with elevated HP

To investigate the impact of various HP on TSP-1 expression, HTM cells were incubated at different HP levels (0, 20, or 60 mmHg) for 48 hours. Expression of TSP-1 was subsequently assessed via WB and IF staining.

Despite the maximum TSP-1 expression observed at 20 mmHg in WB results, statistical analysis showed no significant difference (figure 13A and 13B). However, the IF microscopy results revealed that HTM cells treated with 20 mmHg showed significantly stronger TSP-1 (MFI/cell) compared to 0 mmHg ($p < 0.05$), as shown in figure 13C and 13D.

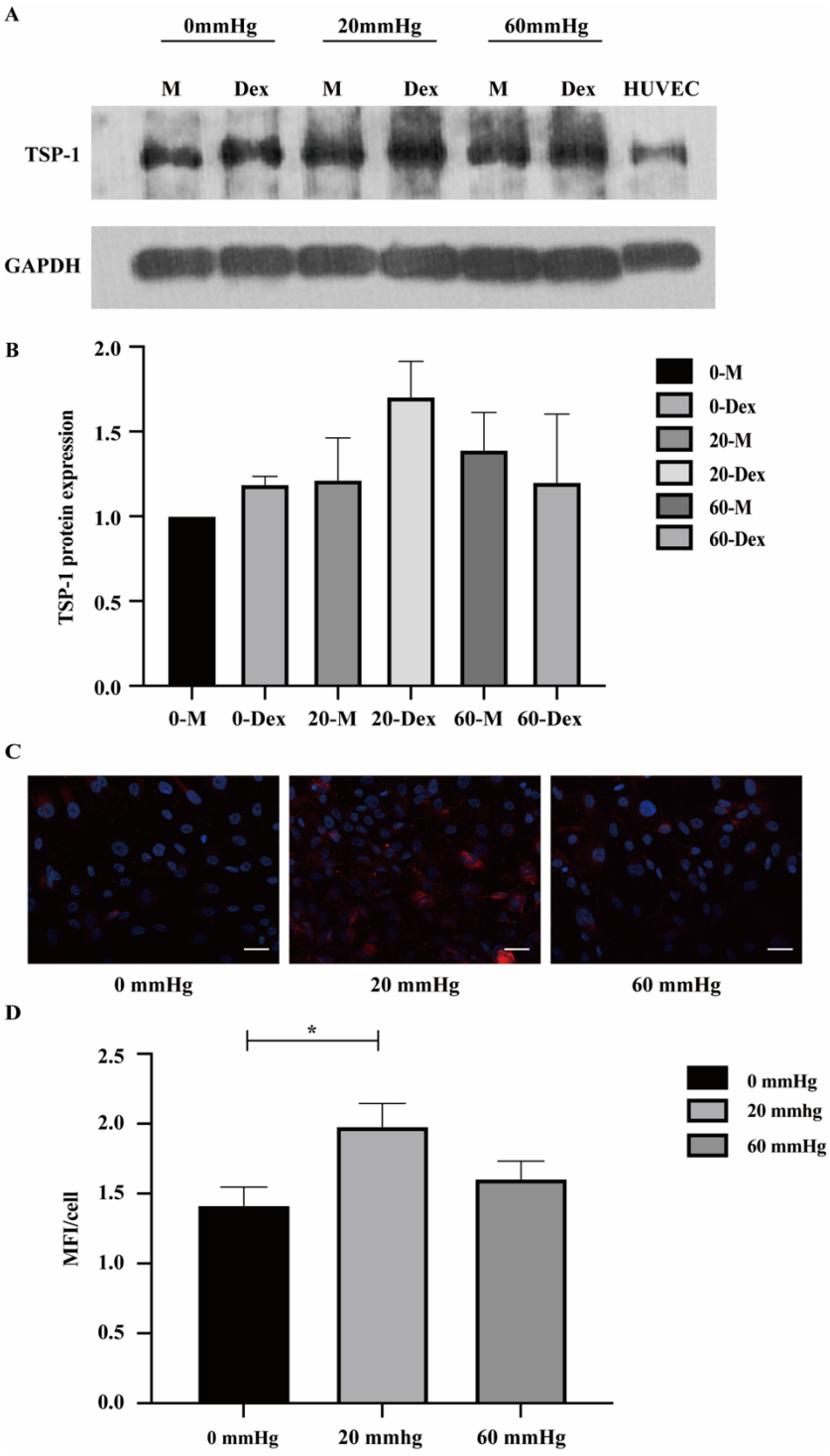

Figure 13. TSP-1 protein expression in HTM cells.

(A) WB images show the expression of TSP-1 protein in HTM cells under varying stimulations. (B) Bar graph illustrating the level of TSP-1 protein with a mean ± SEM, n = 3 independent experiments. (C) Expression of TSP-1 in HTM cells corresponding to various HP levels. Scale bar = 50 μm. (D) Bar graph displays the expression level of TSP-1 in HTM cells (MFI/cell) with a mean ± SEM, n = 3 independent experiments. Kruskal-Wallis' test, *$p < 0.05$.

3.6 CD47 expression in HTM cells after exposure to Dex in combination with elevated HP

The expression of CD47 protein was determined under exposure to Dex in combination with elevated HP (0, 20 or 60 mmHg) through WB and IF staining in HTM cells. The results showed an increase in the protein expression of CD47 when HP was elevated. Additionally, Dex induced the expression of CD47 protein, particularly at 20 mmHg and 60 mmHg (figure 14A and 14B). Despite the maximum CD47 expression observed at 20 mmHg in WB results, statistical analysis showed no significant difference (figure 14A and 14B). Meanwhile, the results of IF microscopy exhibited a similar trend, although no significant differences were observed, as depicted in figures 14C and 14D.

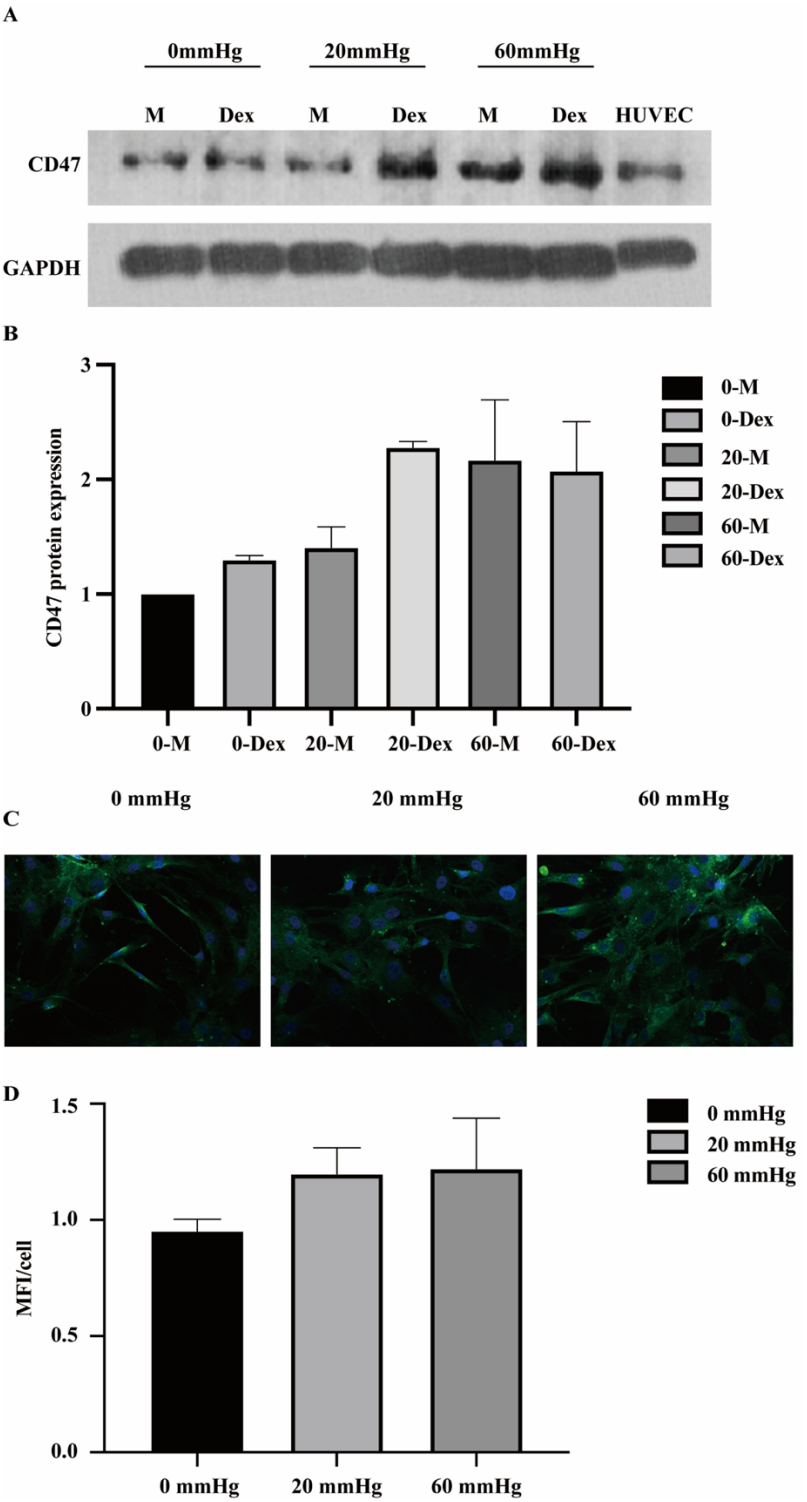

Figure 14. Expression of CD47 protein in HTM cells following exposure to Dex in combination with elevated HP

(A) WB images of CD47 protein expression in HTM cells under different stimulations. (B) Bar chart displays the protein level of CD47. Data are presented as mean ± SEM, n = 3 independent experiments. (C) CD47 expression in HTM at different HPs. Scale bar = 50 μm. (D) Bar chart displaying the expression level of CD47 in HTM cells (MFI/cell). Data are presented as mean ± SEM, n = 3 independent experiments. Kruskal-Wallis' test.

3.7 Viability of HTM cells after stimulation with TSP-1 protein, P4N1 or monoclonal antibody (mAb) targeting CD47

To assess the viability of HTM cells after different stimulations (TSP-1 protein, P4N1 or anti-CD47 mAb), the MTT assay was conducted. HTM cells were cultured with a CD47 binding peptide of TSP-1, P4N1 (1, 2.5, 5 and 10 μM), the scrambled control, P4G1 (1, 2.5, 5 and 10 μM), or anti-CD47 mAb (2, 5, 10 and 15 μg/ml). The results showed that the viability of HTM cells was lower with the concentration of P4N1 at 5 μM ($p < 0.05$) and of 10 μM ($p < 0.01$) compared to medium group (figure 15A). There were no noteworthy variations found in the scrambled control group (P4G1). In the anti-CD47 mAb (B6H12) group, there was also no discernible correlation between cell viability and increasing concentrations (figure 15B). In a subsequent experiment, TSP1 protein (1 μg/ml), P4N1 (10 μM), P4G1 (10 μM), CD47 (5 μg/ml) and co-culture with CD47 were used.

In the additional experiments, there was a significant reduction in the viability of HTM cells in both the TSP-1 protein group and the P4N1 group compared to the medium group ($p < 0.0001$ and $p < 0.001$). Conversely, cell viability significantly increased following treatment with the neutralizing antibody targeting CD47 and TSP-1 protein co-stimulation compared to TSP-1 protein alone ($p < 0.05$). In the group treated with the anti-CD47 mAb and P4N1 co-stimulation, cell viability increased but did not reach a significance compared to the P4N1 group (figure 15C).

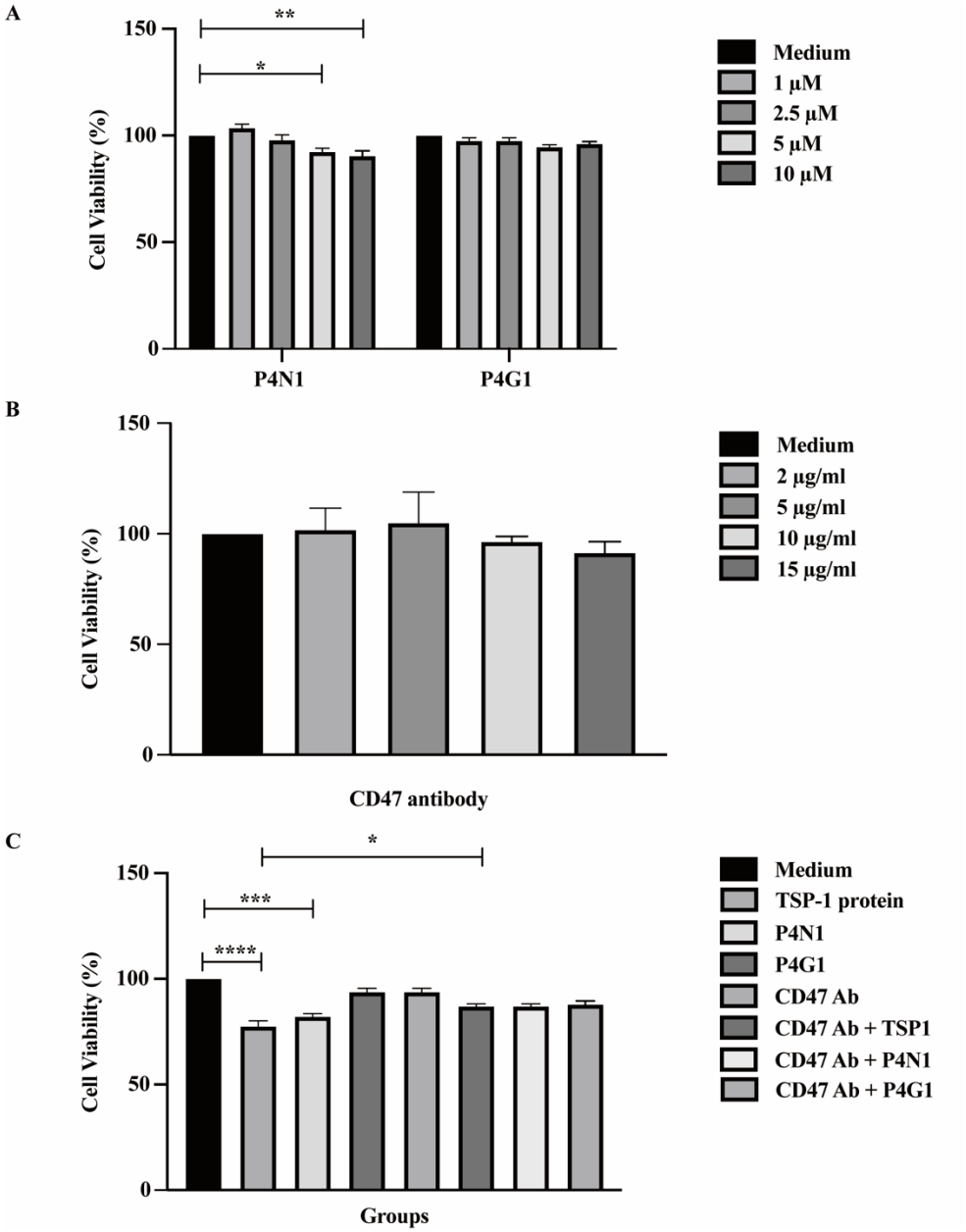

Figure 15. Viability of HTM cells (%) after stimulation with TSP-1 protein, TSP-1 peptide (P4N1), or mAb targeting CD47.

(A) Cell viability (%) in medium and under varying concentrations of P4N1 (1, 2.5, 5 and 10 µM) or P4G1 (1, 2.5, 5 and 10 µM). (B) The viability (%) of HTM cells was analyzed following treatment with anti-CD47 antibodies at different concentrations (2, 5, 10 and 15 µg/ml). (C) The percentage of viable HTM cells was evaluated under different stimulations, including TSP-1 protein (1 µg/ml), P4N1 (10 µM), P4G1 (10 µM), CD47 Ab (5 µg/ml), CD47 Ab (5 µg/ml) and TSP-1 protein (1 µg/ml), CD47 Ab (5 µg/ml) and P4N1 (10 µM), CD47 Ab (5 µg/ml) and P4G1 (10 µM). The data are mean ± SEM (n = 6 independent experiments). Statistical significance between different treatments (*$p < 0.05$, **$p < 0.01$, ***$p < 0.001$, ****$p < 0.0001$). Figure 7A was determined by Two-Way ANOVA (Tukey). Figure 7B and 7C were determined by Kruskal-Wallis' test.

3.8 Viability of HTM cells after exposure of HTM cells to Dex

The impact of Dex on the viability of HTM cells was assessed using the MTT assay at different concentrations of Dex (0, 100, 1000, and 10000 nM) for 48 hours. Dex-treated groups showed a notable decline in HTM cell viability in a concentration-dependent manner starting from 100 nM (figure 16), while no significant difference was observed compared to the control group treated with the medium alone.

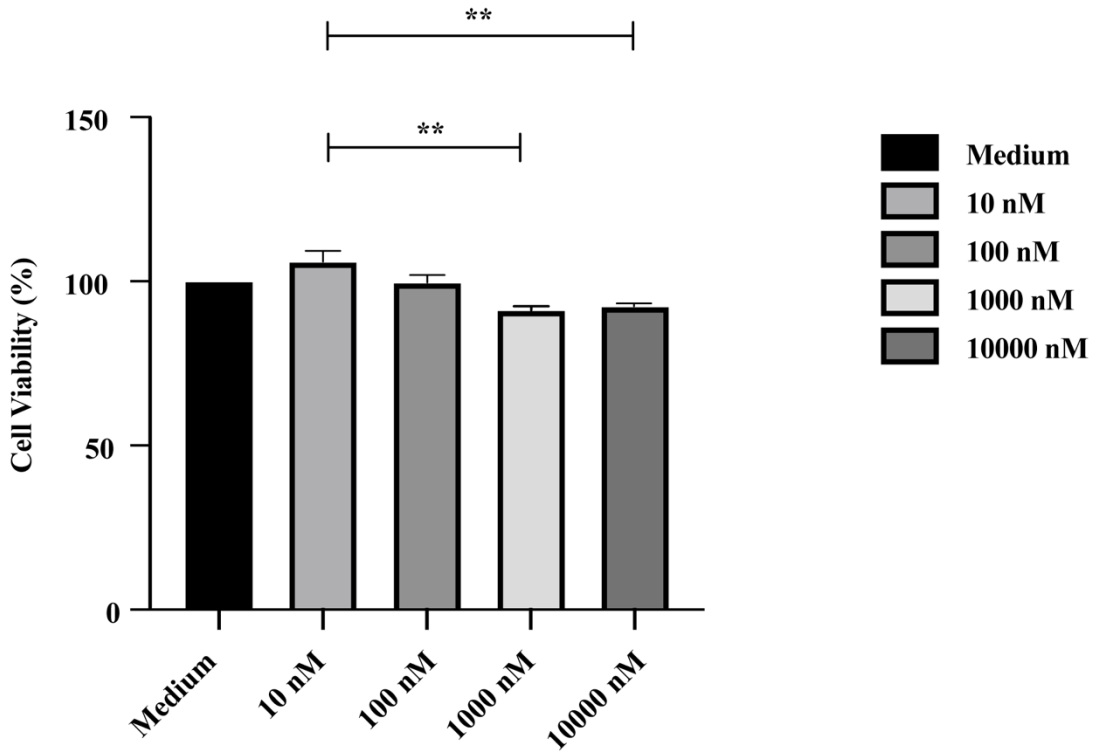

Figure 16. Viability of HTM cells (%) after incubate with Dex in different concentrations.

Cell viability of HTM cells in the presence of 0, 10, 100, 1000 and 10000 nM Dex for 24 hours. Values represent with mean ± SEM (n = 6). Significant differences were determined using Kruskal-Wallis' test (**p < 0.01).

3.9 NO production of HTM cells after stimulation with TSP-1 protein, P4N1 or mAb targeting CD47

To determine the production of NO following various stimulations, an NO assay of the HTM cell supernatants was performed. The HTM cells were cultured with P4N1 (at

concentrations of 1, 2.5, 5, 10, or 20 μM), P4G1 (1, 2.5, 5, 10, or 20 μM), or CD47 Ab (2, 5,10, 15, or 20 μg/ml). Additionally, CD47 Ab (2 μg/ml) was co-cultured with P4N1 at different concentrations (1, 2.5, 5, 10, or 20 μM).

The experiments exhibited a concentration-dependent reduction of NO levels after coculture with P4N1 (P4N1 1 μM: $p < 0.05$; 2.5 μM: $p < 0.01$; 5, 10 and 20 μM: $p < 0.0001$). Moreover, administration of 2 μg/ml anti-CD47 mAb resulted in no change in NO production; however, further administration of P4N1 peptide (2 μg/ml anti-CD47 mAb + 5 μM P4N1: $p < 0.05$; 10 μM P4N1: $p < 0.001$; 20 μM P4N1: $p < 0.05$) resulted in a significant decrease of NO in the supernatants of HTM cells.

To determine the effect of pressure, HTM cells were cultured at 0, 20 or 60 mmHg for 48 hours, and NO levels were subsequently measured in the supernatants. A significant reduction in NO levels was observed when samples were exposed to an elevated pressure of 60 mmHg (Medium 0 mmHg *vs* Medium 60mmHg: $p < 0.05$). A significant reduction in NO level also occurred after incubation at elevated pressure (60 mmHg) and concomitant administration of the P4G1 control peptide (P4G1 0 mmHg *vs* P4G1 60mmHg: $p < 0.01$). Furthermore, incubation with the neutralizing antibody against CD47 resulted in a significant reduction in NO under elevated hydric pressure (anti-CD47 mAb 0 mmHg *vs* anti-CD47 mAb 60mmHg: $p < 0.05$). In summary, the data show that although the neutralizing anti-CD47 mAb leads to a slight increase in NO concentration when used against P4N1, it is not able to compensate for the NO reduction induced by the pressure increase triggered NO reduction.

In various animal models, research has shown that the use of the neutralizing mAb targeting CD47 can alter the relationship between NO and arginase. Moreover, macrophages exhibit lower NO levels and increased arginase levels under pressure (Wang, 2020). Consequently, a subsequent experiment was conducted to examine how CD47 neutralization impacts the NO/arginase ratio. Arginase is an enzyme that converts L-arginine to L-ornithine and urea. The arginase activity assay utilized in this study was modified from Schimke's method (Corraliza et al., 1994). As depicted in figure 18, there

were marginal variances observed in the results when different pressure and stimulations were applied.

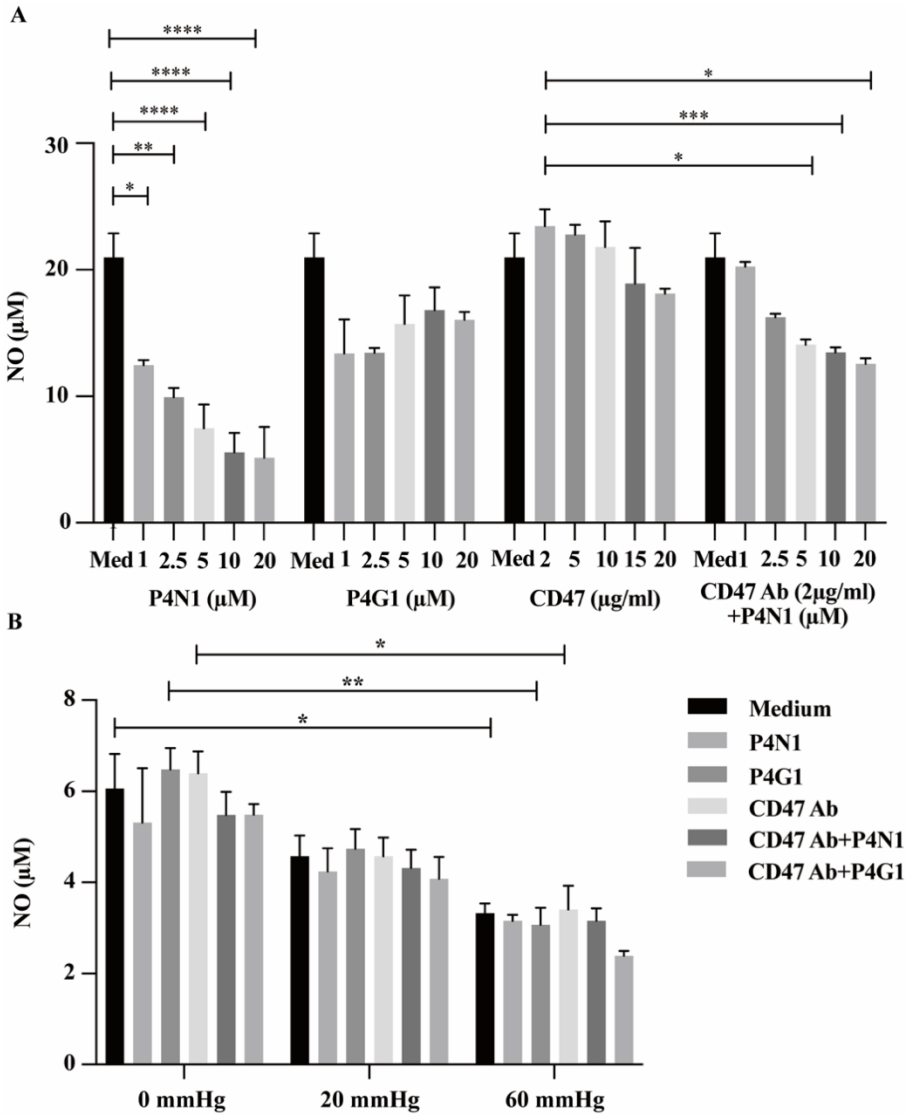

Figure 17. Production of NO in HTM cells after stimulation with TSP-1 protein, TSP-1 peptide (P4N1) or mAb targeting CD47

(A) NO levels (μM) in medium, P4N1 (1, 2.5, 5, 10 and 20 μM), P4G1 (1, 2.5, 5, 10 and 20 μM), anti-CD47 mAb (2, 5, 10, 15 and 20 μg/ml) or 2 μg/ml anti-CD47 mAb with P4N1 (1, 2.5, 5, 10 and 20 μM). (B) NO levels (μM) in different HP and medium, P4N1 (1 μM), P4G1 (1 μM), anti-CD47 mAb (2 μg/ml), anti-CD47 mAb (2 μg/ml) and P4N1 (1 μM), anti-CD47 mAb (2 μg/ml) and P4G1 (1 μM). The data are mean ± SEM (n = 3 independent experiments). Statistical significance between different treatments (*$p < 0.05$, **$p < 0.01$, ****$p < 0.0001$). Two-way ANOVA (Tukey). Med = medium. NO = nitric oxide. CD47 = cluster of differentiation 47. P4N1 = CD47-ligand TSP-1 peptide. P4G1 = CD47-ligand TSP-1 peptide negative control. HTM = human trabecular meshwork.

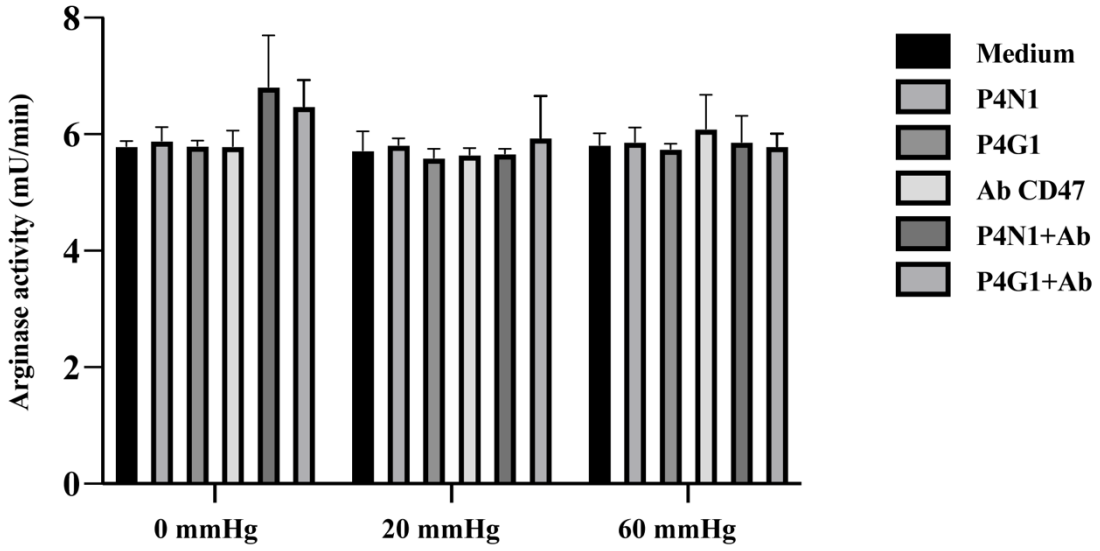

Figure 18. Arginase activity (mU/min) in different stimulations.
Arginase activity (mU/min) in medium, P4N1 (1 μM), P4G1 (1 μM), anti-CD47 mAb (2 μg/ml), anti-CD47 mAb (2 μg/ml) and P4N1(1 μM) or anti-CD47 mAb (2 μg/ml) and P4G1 (1 μM) treated HTM cells under different HP (n = 3 independent experiments). CD47 = cluster of differentiation 47. P4N1 = CD47-ligand TSP-1 peptide. P4G1 = CD47-ligand TSP-1 peptide negative control. HTM = human trabecular meshwork. Two-way ANOVA.

3.10 Expression of fibronectin after stimulation with TSP-1 protein, P4N1 or mAb targeting CD47

To determine the influence of TSP-1 and CD47 on fibronectin, IF was performed. The result showed that in TSP-1 protein group, P4N1 group and CD47 antibody group fibronectin exhibited higher levels of expression than to the medium group. In the TSP-1 protein and anti-CD47 mAb co-culture group, the expression level of fibronectin was significantly higher ($p < 0.05$) than the medium group.

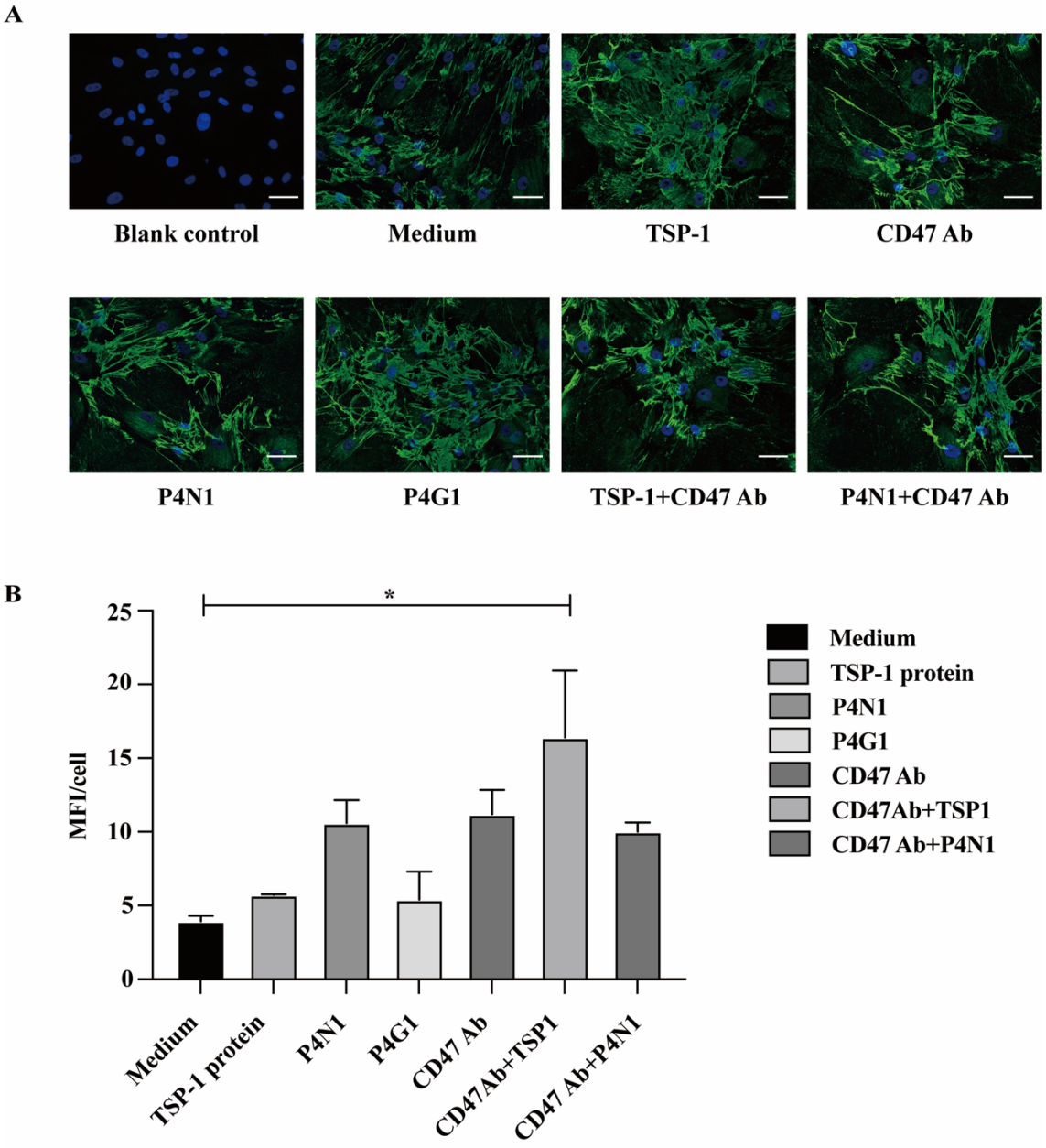

Figure 19. Expression of fibronectin in HTM cells after stimulation with TSP-1 protein, P4N1 or mAb targeting CD47.

(A) Exemplary expression of fibronectin in HTM cells across different groups. Scale bar = 50 µm. (B) Bar chart displaying the expression level of fibronectin in HTM cells (MFI/cell). Data are presented as mean ± SEM, n = 3. One-way ANOVA. *$p < 0.05$.

3.11 Effect of stimulation with Dex on motility in HTM cells

HTM cell migration was quantified using an *in vitro* scratch assay. The degree of motility was assessed by calculating the percentage of the blank area. A higher percentage indicates decreased cell motility, while a lower percentage suggest increased cell motility. Figure 20 illustrates the extent of empty space between the medium group and Dex (100 nM) group after the scratch. Initially (at 0 hour), there was no significant difference between the two groups. Similarly, after 24 hours, there was also no difference between the two groups, indicating that Dex treatment has no influence on the cell migration.

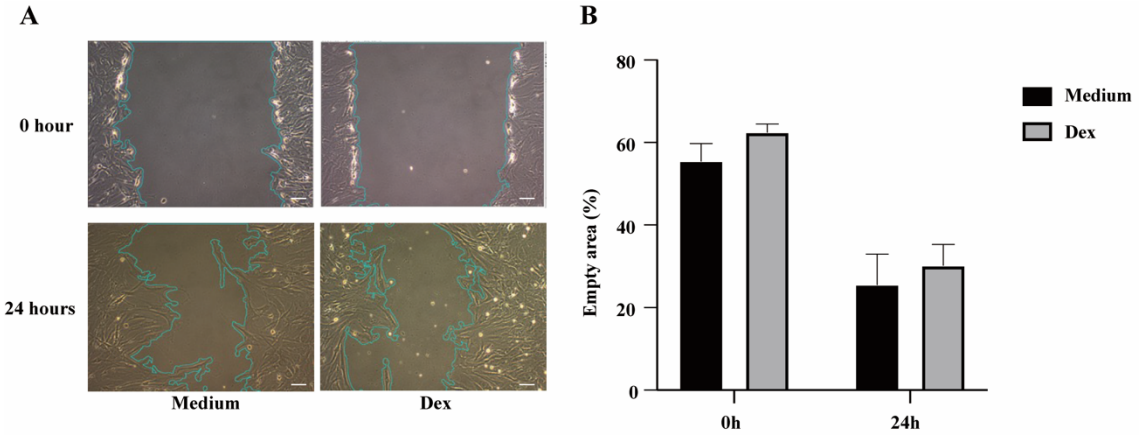

Figure 20. The cell motility of HTM cells.
(A) Representative photographs of the medium and Dex treatment groups at 0 h and 24 hours. The empty area is between the blue lines on both sides. Scale bar = 25 μm. (B) A histogram indicating the percentage of empty area. The data are depicted as mean ± SEM (n = 3). No significant difference (Kruskal-Wallis' test). Dex = dexamethasone. HTM = human trabecular meshwork.

4 Discussion

Glaucoma, is a complex ocular disorder characterized by progressive optic nerve damage and visual field loss, which remains a significant global health problem. The main theory of glaucoma pathogenesis lies in the balance of intraocular pressure, which is largely controlled by the function of the trabecular meshwork. This unique tissue serves as the primary outflow pathway for aqueous humor and plays a pivotal role in regulating intraocular pressure and maintaining ocular homeostasis. Perturbations in the structure and functionality of the trabecular meshwork can lead to inadequate aqueous humor drainage of aqueous humor, leading to elevated intraocular pressure and subsequent optic nerve damage. TSP-1 is an ECM protein which is involved in many cellular processes and is induced by growth factors and cellular stresses (Murphy-Ullrich and Downs, 2015). CD47 is one of its receptors, and it is expressed in multiple human cells. The interaction between TSP-1 and CD47 has wide-ranging effects on cell behavior, immune responses, and disease processes.

In this study, the interaction between TSP-1 and the CD47 receptor in HTM cells is investigated. Conditions of elevated intraocular pressure were mimicked using the pressure chamber system (Böhm et al., 2016). The impact of Dex was also explored, as steroids may contribute to an increase in intraocular pressure. The influence of TSP-1 and CD47 on viability, nitric oxide production, expression of extracellular matrix was investigated.

4.1 Biological function, isolation and morphology of HTM cells

HTM cells are vital components of the conventional outflow pathway, serving as the primary route for aqueous humor outflow in the human eye (Stamer and Clark, 2017). HTM cells function as biological filters, removing cellular debris and pigment particles by exhibiting macrophage-like activity within the inner TM (Stamer and Clark, 2017). Additionally, HTM cells generate resistance to maintain IOP. HTM cells produce

numerous ECM proteins as well as their associated degradation enzymes to support ongoing remodeling (Keller et al., 2018). For this study, HTM tissues were isolated from donor corneoscleral rims and further cultured as described previously (Keller et al., 2018). HTM is composed of four regions that are difficult to isolate and hard to culture each region separately. Therefore, the culture of HTM cells is usually a cell mixture of the four regions. During the culturing of HTM cells, their morphology remained stable for 48 hours when stimulated by either the TSP-1 protein, the CD47-ligand-TSP-1 peptide, also known as P4N1 or the anti-CD47 mAb, as observed through light microscopy. Furthermore, the elevated HP did not alter the morphology of HTM cells.

4.2 Production of α-SMA, fibronectin and myocilin in isolated HTM cells following exposure to Dex

Morphology alone is not sufficient to identify TM cells, so further identification methods are required. To date, there are no known surface markers or intracellular markers that can effectively differentiate HTM cells from other types of cells. The identification of HTM cells used in the present study is based on their property of displaying elevated expression of α-SMA, fibronectin and myocilin after being induced by glucocorticoids (Clark et al., 2001; Stamer and Clark, 2017)

Myofibroblasts express a-SMA, a protein involved in wound healing and remodeling of tissue. Previous research has demonstrated that α-SMA expression, particularly after exposure to Dex, is a hallmark of HTM (Yemanyi et al., 2020). Dex can stimulate the synthesis of α-SMA in HTM cells by activating the TGF-β signaling cascade. TGF-β, a cytokine involved in various cellular processes such as cell differentiation and proliferation, functions as a profibrotic signal for cultured TM cells (Stamer and Clark, 2017). Fibronectin plays a role in cellular adhesion and migration and serves as one of the key ECM proteins in the TM. The production of fibronectin in HTM cells can be stimulated by Dex (Watanabe et al., 2021). Myocilin is expressed in HTM cells at higher

levels compared to neighboring cells but its expression decreases during the cell culturing process (Fautsch et al., 2005). However, the expression of myocilin is strongly upregulated when HTM cells are treated with glucocoticoids but not in neighboring cells (Polansky et al., 2000). Therefore, glucocoticoids induced myocilin expression is considered the most common and reliable way to identify HTM cells. The results showed this phenomenone (figure 10), in line with results reported by other researcher (Joe et al., 2011).

4.3 Expression of TSP-1 in cultivated HTM cells

TSP-1 is a glycoprotein produced by many cell types. In this study, the expression of TSP-1 in HTM cells was demonstrated by IHC, IF and WB. In a previous study, TSP-1 expression was found to be increased in one third of POAG eyes as examined by immunostaining (Flügel-Koch et al., 2004). *In vitro,* HTM cells from healthy donor eyes were cultured and treated with either Dex or TGF-β1. WB analysis revealed that TSP-1 protein was undetectable in the normal group, but TSP-1 protein was detected after treatment with Dex or TGF-β1. TSP-1 was not detected by Northern Blotting in untreated HTM cells from two donors. However, treatment with Dex or TGF-β1 for three days resulted in the detection of TSP-1 expression (Flügel-Koch et al., 2004).

In the present study, HUVECs were used as a positive control for TSP-1 expression, as the constitutive TSP-1 protein expression in HUVEC was previously reported (Ridnour et al., 2005). Three HTM cell lines were used to detect TSP-1 expression by WB. TSP-1 expression was positive in all cell lines without any stimulation (figure 13). Upon stimulation of HTM cells with Dex (100 nM) for 48 hours, a stronger TSP-1 expression was observed (figure 13). These results was similar to a previous study (Shan et al., 2017). However, another study reported decreased TSP-1 levels in HTM cells after stimulation with 100 nM Dex for 2 weeks (Liu et al., 2003). One difference between the current study and the aforementioned study is the length of stimulation time. It could be speculated that

a shorter stimulation time could induce the stronger expression, whereas long-term cultures of 14 days establish a kind of counter-regulation. In another study, TSP-1 mRNA expression levels were observed to increase after 8 hours of stimulation in HUVECs with Dex (600 nM) and decrease after 22 hours (Logie et al., 2010). Another study reported that TSP-1 is a glucocorticoid responsive protein in human peripheral blood mononuclear cell (PBMC) (Barclay et al., 2016). The stimulation with Dex may lead to the activation of intracellular signaling pathways that subsequently promote TSP-1 gene and protein levels. As TSP-1 is found to be increased in glaucomatous eyes its overexpression may contribute to the development and progression of glaucoma (Flügel-Koch et al., 2004).

Previous research has demonstrated that several conditions can cause an upregulation of TSP-1 expression in cultured HTM cells. Chronically increased endoplasmic reticulum (ER) stress in HTM tissues or cells, caused by aging, oxidative stress, and glucocorticoid treatment, has been identified as a contributing factor in glaucoma (Peters et al., 2015). Additionally, TSP-1 expression may also increase in the trabecular meshwork when subjected to mechanical stress, such as stretch or shear stress. This may be due to the activation of signaling pathways resulting in increased transcription of the TSP-1 gene and subsequent expression of TGF-β (Murphy-Ullrich and Downs, 2015). TSP-1 expression is regulated by various cytokines and growth factors, such as TGF-β and TNF-α (Fairaq et al., 2015; Flügel-Koch et al., 2004).

In conclusion, the changes in TSP-1 protein levels in HTM cells after the pressure and Dex stimulation, as shown in this work, are likely due to complex cellular signaling regulatory mechanisms.

4.4 Expression of CD47 in cultivated HTM cells

The expression of CD47 in HTM cells was confirmed through flow cytometry and IF in this study. To assess the expression changes of CD47 under different pressure conditions with or without Dex, WB was employed. The results indicated no statistically significant

differences in CD47 expression, which aligns with findings from a previous study, where HTM cells were treated with 500 nM Dex for 5 days. Subsequent microarray analysis did not reveal any significant changes in CD47 mRNA expression, which was further validated by flow cytometry (Faralli et al., 2019a). Currently, there are no other studies exploring the expression changes of CD47 under different pressure conditions.

4.5 The influence of TSP-1 and CD47 on NO production

TSP-1 plays a crucial role in regulating nitric oxide signaling in vascular physiology (Isenberg et al., 2008a). CD47 ligation has also been found to effectively inhibited NO-induced sGC and cGMP flux in both vascular smooth muscle cells (VSMCs) and endothelial cells (Isenberg et al., 2008a). Nanomolar concentrations of TSP-1 binding to CD47 were found to inhibit eNOS activation, resulting in a reduction in NO production in endothelial cells (Bauer et al., 2010). In arterial, skeletal muscle, and lung tissue, endothelial cells from tissue of TSP-1-null and CD47-null mice both exhibited elevated eNOS activity (Bauer et al., 2010). The present study conducted herein found that the use of exogeneous TSP-1 peptide decreased NO production in HTM cells, while the anti-CD47 antibody increased it. The CD47-ligand-TSP-1 peptide, also known as P4N1, was cultured with a CD47 antibody with HTM cells. The results indicate that the CD47 antibody effectively blocked TSP-1 peptide P4N1 from inhibiting NO production, consistent with the literature (Kale et al., 2021). In HTM cells, the binding of exogeneous TSP-1 to CD47 may inhibit eNOS and iNOS production, further decreasing NO production. Down-regulation of eNOS activity and a reduced availability of NO are associated with POAG (Patel et al., 2021).

NO is a naturally occurring gas in mammals, that is essential for the regulation of vascular health and cardiovascular disease. NO is produced by three isoforms of NOS: neuronal (nNOS), endothelial (eNOS), and inducible (iNOS). Evidence suggests that HTM cells

express both eNOS and iNOS, while nNOS is absent (Fernández-Durango et al., 2008; Sierra et al., 2014).

It is widely accepted that NO regulates a feedback loop in the conventional outflow pathway to control IOP. Elevated IOP could result in increased endothelial shear stress, according to previous research (McDonnell et al., 2020). Therefore, eNOS activation in SC cells generates additional NO, which diffuses into the HTM, causing tissue relaxation and IOP reduction (Reina-Torres et al., 2021). Several studies have suggested a correlation between dysregulated NO synthesis or downstream signaling and the development or progression of glaucoma (Doganay et al., 2002; Galassi et al., 2004). In this study, as HP increased, NO levels in HTM cells significantly decreased. One possible explanation is that increasing pressure led to a reduced expression of eNOS and iNOS, which ultimately resulting in reduced NO (Förstermann and Li, 2011). However, another study conducted perfusion on anterior segments of human donor eyes, examining the influence of increased perfusion pressure on NO levels within the perfusate. They found a significant increase in iNOS concentration in the TM due to a rise in perfusion pressure in eyes donated by humans (Schneemann et al., 2003). Another potential explanation is the disruption of the balance between arginase and NO. Arginase inhibits the production of NO via several potential mechanisms. Elevated arginase activity can affect the synthesis and stability of iNOS, compete for the L-arginine substrate and uncouple NOS, which results in less NO generation (Durante et al., 2007). Moreover, arginase can inhibit iNOS-mediated NO by generating urea (Durante et al., 2007). Therefore, arginase activity was also assessed in this study. The data indicate that the elevated NO/arginase ratio observed in the present study is most probably caused by an increase in NO during experiments, rather than arginase decrease. Furthermore, the results indicate that the neutralizing antibody targeting CD47 is unable to reverse the decrease in NO levels caused by increased HP.

4.6 The influence on HTM biological cell functions by CD47, TSP-1 and Dex

MTT is a substance used in colorimetric assays to assess cell viability. Viable cells with active metabolism are able to convert MTT into a purple formazan product enabling assessment of viable cells. In the present study, exogenous TSP-1 protein or peptide and anti-CD47 antibody were employed to treat HTM cells, leading to decreased viability in the TSP-1 group. Contrastingly, in the group pre-treated with anti-CD47 mAb followed by treatment with TSP-1 protein or peptide, cell viability exhibited an augmentation compared to the group treated solely with TSP-1 protein or peptide. The results suggest that TSP-1 and CD47 are involved in the cell viability of HTM cells.

In the present study HTM cells were also treated with different concentrations (10, 100, 1000 and 10,000 nM) Dex for 48 hours. Results showed that concentrations of 10 nM or 100 nM had no significant effect, while concentrations of 1000 nM or 10,000 nM significantly reduced cell viability. These findings are consistent with previous research, indicating that low concentrations of Dex do not affect HTM cell viability (Sharma et al., 2013). In the previous study, the authors observed a dose-dependent decrease in mitochondrial dehydrogenase activity with high concentrations of Dex (Sharma et al., 2013). This indicates that at elevated concentrations, Dex is involved in cell death through the mitochondrial apoptosis pathway. Additionally, a scratch assay was performed after treatment with 100 nM Dex (figure 20). However, no significant differences were observed compared to the medium group after 24 hours.

An influence of TSP-1 and CD47 on the viability of primary murine lung-derived endothelial cells had been shown by another group (Isenberg et al., 2008b). The study revealed both the TSP-1-null and CD47-null mice had significantly lower cell death in both muscle and bone marrow after 12 hours of 25-Gy hindlimb irradiation. Furthermore, null mice showed survival and enhanced proliferative capacity of vascular cells after *in vitro* irradiation. Overall, these findings suggest a potential role for both TSP-1 and CD47 in influencing cell death.

Possible mechanisms for the influence of TSP-1 and CD47 on cell viability include modulation of cell apoptosis or the cell cycle. In a previous study, the TSP-1-CD47 signaling pathway expedited replicative senescence and induced concurrent cell cycle arrest in endothelial cells (Gao et al., 2016). The insufficiency in endothelial cells markedly enhanced their angiogenic capacity and mitigated their replicative senescence. Furthermore, the lack of CD47 inhibits the activation of cell cycle inhibitors and increases the expression of cell cycle promoters, promoting cell cycle progression (Gao et al., 2016). Additionally, the CD47 binding domain of TSP1 induces apoptosis in human T cells (Lamy et al., 2003).

Another potential explanation is that TSP-1, via CD47, induces mitochondrial dysfunction, leading to cell death (Roberts and Isenberg, 2021). In a study, the treatment of human T cells with TSP-1 protein or TSP-1-derived peptides that specifically bind to CD47 resulted in cell death (Manna and Frazier, 2003). When leukemia cells were exposed to TSP-1 or its C-terminal domain (which interact with CD47) it induced a disruption in mitochondrial membrane potential, heightened generation of mitochondrial reactive oxygen species (ROS), and enhanced cell death (Saumet et al., 2005). Moreover, low concentrations of NO and cyclic adenosine monophosphate (cAMP) enhance the stimulation of mitochondrial biogenesis (Roberts and Isenberg, 2021). As previously stated, TSP-1 can inhibit the production and signaling of NO through CD47.

HTM is the major structure in the fluid pathway to regulate IOP. TM cells are depleted with age and continuous exposure to cytotoxic agents. As a result of disruption of the trabecular meshwork beams, aqueous humor outflow is impaired, eventually leading to increased intraocular pressure (Alvarado et al., 1984). Apoptosis or abnormal activity in HTM can lead to abnormal aqueous humor outflow, thereby increasing intraocular pressure and elevating the risk of glaucoma. This study suggests that the TSP-1/CD47 signaling pathway affects the viability of HTM cells, which may contribute to an increased risk of glaucoma. Dex does not affect the activity and migration of HTM cells

at low concentrations. However, the long-term effects of Dex have not been investigated here and require further experiments.

4.7 TSP-1/CD47 signaling modulate expression of fibronectin in HTM cells

The ECM of the TM is thought to act as a reservoir of latent growth factors and other small regulatory molecules. However, if the ECM becomes saturated, such as in response to elevated pressure, the regulatory molecules can gain access to the outflow channels and modify the resistance accordingly. The ECM of the TM provides a microenvironment with unique biomechanical characteristics that are crucial for its biological function. Previous research has shown that fibronectin accumulates in glaucomatous trabecular meshwork (Faralli et al., 2019b). The current study found that the expression of fibronectin increased in the groups treated with TSP-1 protein, P4N1, and anti-CD47 mAb groups. The highest expression level was observed when TSP-1 protein and anti-CD47 mAb were used in combination to culture HTM cells.

Evidence has suggested a direct interaction between fibronectin and TSP-1 secreted by endothelial cells (Lahav et al., 1982). In these studies, chemically cross-linked fibronectin was adsorbed onto glass coverslips, co-incubated with platelets, and it was found that TSP-1 was associated with the fibronectin-coated coverslips. TSP-1 can influence the structure and function of the ECM through direct interactions and indirect effects on other components secreted by cells. Fibronectin can bind to the N-terminal domain of TSP-1, as well as to protein hydrolytic fragments containing EGF-like repeat sequences and TSR (Dardik and Lahav, 1999). The binding of fibronectin to TSP-1 can also stabilize a calcium-dependent structure, preventing the degradation of TSP-1 (Dardik and Lahav, 1999).

Moreover, TSP-1 has the ability to activate latent TGF-β, which may increase the expression of fibronectin (Sweetwyne and Murphy-Ullrich, 2012). TGF-β is known to play a central role in the pathology of glaucoma. Elevated expression of TGF-β2 in the

aqueous humor has been observed in glaucoma patients, and increased levels of TGF-β1 and TSP-1 has been found in the plasma of POAG patients are also increased (Kuchtey et al., 2014; Tripathi et al., 1994). In HTM cells treated with TGF-β2, fibronectin secretion was increased (Fleenor et al., 2006).

Currently there is limited research provided on the interaction between CD47 and fibronectin or ECM. However, a previous study observed a significant increase in tumor-associated ECM protein tenascin C (TNC) both *in vitro* and *in vivo* in CD47 knockout conditions (Ma et al., 2019). In contrast, in another study, found that while both TSP-1 and CD47 were upregulated in mouse kidney injury. Blocking or eliminating CD47 mediated signaling actually mitigated renal fibrosis and decreased expression of fibronectin (Julovi et al., 2020). This finding contradicts the results of the current study, which observed an increase in fibronectin expression after CD47 blocking. However, further examination of additional ECM components and an in-depth exploration of potential mechanisms are still required for the current study.

5 Summary

Human trabecular meshwork (HTM) cells play a crucial role in the outflow of aqueous humor. The identification of these cells for this study was achieved through the use of markers such as alpha-smooth muscle actin (α-SMA), fibronectin, and myocilin, particularly under dexamethasone (Dex) stimulation.

The study also examined the expression of thrombospondin-1 (TSP-1) and CD47 in cultured HTM cells, noting an increase in TSP-1 and CD47 levels under Dex stimulation. No statistically significant differences in TSP-1 and CD47 expression levels were observed under Dex stimulation and additionally increased pressure.

Exposure to TSP-1 protein and the CD47 binding peptide of TSP-1 (P4N1) led to a significant decrease in HTM cell viability, while co-stimulation with anti-CD47 monoclonal antibody (mAb) increased viability. The P4N1 peptide also showed a concentration-dependent reduction in nitric oxide (NO) production. Interestingly, co-culture with anti-CD47 mAb and P4N1 peptide resulted in a significant decrease compared to the group solely with anti-CD47 mAb in NO levels, emphasizing their antagonistic effect. Moreover, elevated pressure conditions contributed to a notable reduction in NO levels, highlighting the complex interactions between TSP-1, CD47, and pressure on cellular responses.

The Immunofluorescence analysis indicated elevated fibronectin expression in the TSP-1 protein, P4N1, and CD47 antibody groups. Notably, the co-culture of TSP-1 protein and CD47 antibody showed a significant increase in fibronectin levels, suggesting a collaborative influence.

Future studies should expand coverage to encompass a more comprehensive understanding of extracellular matrix (ECM) dynamics in the context of TSP-1 and CD47 interactions and into the intricate signaling pathway involved in the regulatory mechanisms of NO production.

In summary the study provided insights into TSP-1/CD47 signaling in HTM cells, which may lead to a deeper understanding of the pathogenesis of glaucoma.

6 ZUSAMMENFASSUNG

Die Zellen des humanen Trabekelmaschenwerks (HTM) spielen eine entscheidende Rolle beim Abfluss des okulären Kammerwassers. Die Identifizierung dieser Zellen erfolgte durch die Verwendung der Marker alpha-smooth muscle actin (α-SMA), Fibronektin und Myocilin, insbesondere unter gleichzeitiger Behandlung mit Dexamethason (Dex).

Die Studie untersuchte die Expression von Thrombospondin-1 (TSP-1) und cluster of differentiation 47 (CD47) in kultivierten HTM-Zellen. Es wurde ein Anstieg der TSP-1- und CD47-Werte unter Dex-Stimulation festgestellt. Es wurden jedoch keine statistisch signifikanten Unterschiede in den TSP-1- und CD47-Expressionswerten unter Dex-Stimulation und zusätzlich erhöhtem Druck festgestellt.

Die Exposition der HTM-Zellen mit dem TSP-1-Protein oder dem CD47-Bindungspeptid von TSP-1 (P4N1) führte zu einer signifikanten Abnahme der Vitalität der HTM-Zellen. Gleichzeitig führte die Stimulation mit dem monoklonalen Antikörper (mAb) gegen CD47 zu einer Erhöhung der Vitalität. Das P4N1-Peptid verursachte außerdem eine konzentrationsabhängige Verringerung der Stickstoffoxid (NO)-Produktion. Umgekehrt führte die Ko-Kultur mit anti-CD47 mAb und P4N1-Peptid zu einem signifikanten Rückgang der NO-Konzentration im Vergleich zur Gruppe, die ausschließlich mit anti-CD47 mAb kultiviert wurde. Dies unterstreicht ihre antagonistische Wirkung. Erhöhte Druckbedingungen trugen darüber hinaus zu einer deutlichen Verringerung der NO-Werte bei. Dies verdeutlicht die komplexen Wechselwirkungen zwischen TSP-1, CD47 und Druck auf die zellulären Reaktionen. Die Immunfluoreszenzanalyse zeigte eine erhöhte Fibronektin-Expression in den Gruppen mit TSP-1-Protein, P4N1 und CD47-Antikörper. Insbesondere die Co-Kultur von TSP-1-Protein und CD47-Antikörper führte zu einem signifikanten Anstieg der Fibronektinwerte, was auf einen gemeinsamen Einfluss schließen lässt.

Zukünftige Studien sollten die Untersuchungen erweitern, um ein umfassenderes Verständnis der Dynamik der extrazellulären Matrix (ECM) im Zusammenhang mit den Wechselwirkungen zwischen TSP-1 und CD47 sowie der komplizierten Signalwege, die damit einhergehen, zu erlangen.

Zusammenfassend bietet die Studie Einblicke in die TSP-1/CD47-Signalübertragung in Glaukom-HTM-Zellen, die zu einem tieferen Verständnis der Pathogenese des Glaukoms führen können.

7 References

1. Adams, J.C., and Lawler, J. (2011). The thrombospondins. Cold Spring Harb Perspect Biol *3*, a009712.
2. Al-Tubuly, A.A. (2000). SDS-PAGE and Western Blotting. Methods Mol Med *40*, 391-405.
3. Allison, K., Patel, D., and Alabi, O. (2020). Epidemiology of Glaucoma: The Past, Present, and Predictions for the Future. Cureus *12*, e11686.
4. Alvarado, J., Murphy, C., and Juster, R. (1984). Trabecular meshwork cellularity in primary open-angle glaucoma and nonglaucomatous normals. Ophthalmology *91*, 564-579.
5. Barclay, J.L., Petersons, C.J., Keshvari, S., Sorbello, J., Mangelsdorf, B.L., Thompson, C.H., Prins, J.B., Burt, M.G., Whitehead, J.P., and Inder, W.J. (2016). Thrombospondin-1 is a glucocorticoid responsive protein in humans. Eur J Endocrinol *174*, 193-201.
6. Baudouin, C., Kolko, M., Melik-Parsadaniantz, S., and Messmer, E.M. (2021). Inflammation in Glaucoma: From the back to the front of the eye, and beyond. Prog Retin Eye Res *83*, 100916.
7. Bauer, E.M., Qin, Y., Miller, T.W., Bandle, R.W., Csanyi, G., Pagano, P.J., Bauer, P.M., Schnermann, J., Roberts, D.D., and Isenberg, J.S. (2010). Thrombospondin-1 supports blood pressure by limiting eNOS activation and endothelial-dependent vasorelaxation. Cardiovascular research *88*, 471-481.
8. Böhm, M.R.R., Schallenberg, M., Brockhaus, K., Melkonyan, H., and Thanos, S. (2016). The pro-inflammatory role of high-mobility group box 1 protein (HMGB-1) in photoreceptors and retinal explants exposed to elevated pressure. Laboratory Investigation *96*, 409-427.
9. Bradley, J.M., Kelley, M.J., Zhu, X., Anderssohn, A.M., Alexander, J.P., and Acott, T.S. (2001). Effects of mechanical stretching on trabecular matrix metalloproteinases. Investigative ophthalmology & visual science *42*, 1505-1513.
10. Buffault, J., Labbé, A., Hamard, P., Brignole-Baudouin, F., and Baudouin, C. (2020). The trabecular meshwork: Structure, function and clinical implications. A review of the literature. J Fr Ophtalmol *43*, e217-e230.
11. Burke, A.G., Zhou, W., O'Brien, E.T., Roberts, B.C., and Stamer, W.D. (2004). Effect of hydrostatic pressure gradients and Na2EDTA on permeability of human Schlemm's canal cell monolayers. Curr Eye Res *28*, 391-398.
12. Chono, I., Miyazaki, D., Miyake, H., Komatsu, N., Ehara, F., Nagase, D., Kawamoto, Y., Shimizu, Y., Ideta, R., and Inoue, Y. (2018). High interleukin-8 level in aqueous humor is associated with poor prognosis in eyes with open angle glaucoma and neovascular glaucoma. Scientific Reports *8*, 14533.
13. Clark, A.F., Steely, H.T., Dickerson, J.E., Jr, English-Wright, S., Stropki, K., McCartney, M.D., Jacobson, N., Shepard, A.R., Clark, J.I., Matsushima, H., Peskind,

E.R., Leverenz, J.B., Wilkinson, C.W., Swiderski, R.E., Fingert, J.H., Sheffield, V.C., and Stone, E.M. (2001). Glucocorticoid Induction of the Glaucoma Gene MYOC in Human and Monkey Trabecular Meshwork Cells and Tissues. Invest Ophthalmol Vis Sci *42*, 1769-1780.

14. Crouch, D.J., Sheridan, C.M., D'Sa, R.A., Willoughby, C.E., and Bosworth, L.A. (2021). Exploiting biomaterial approaches to manufacture an artificial trabecular meshwork: A progress report. Biomaterials and Biosystems *1*, 100011.
15. Doganay, S., Evereklioglu, C., Turkoz, Y., and Er, H. (2002). Decreased nitric oxide production in primary open-angle glaucoma. European journal of ophthalmology *12*, 44-48.
16. Doughty, M.J., and Zaman, M.L. (2000). Human corneal thickness and its impact on intraocular pressure measures: a review and meta-analysis approach. Surv Ophthalmol *44*, 367-408.
17. Durante, W., Johnson, F.K., and Johnson, R.A. (2007). Arginase: a critical regulator of nitric oxide synthesis and vascular function. Clin Exp Pharmacol Physiol *34*, 906-911.
18. Elzie, C.A., and Murphy-Ullrich, J.E. (2004). The N-terminus of thrombospondin: the domain stands apart. Int J Biochem Cell Biol *36*, 1090-1101.
19. Fairaq, A., Goc, A., Artham, S., Sabbineni, H., and Somanath, P.R. (2015). TNFα induces inflammatory stress response in microvascular endothelial cells via Akt- and P38 MAP kinase-mediated thrombospondin-1 expression. Mol Cell Biochem *406*, 227-236.
20. Faralli, J.A., Desikan, H., Peotter, J., Kanneganti, N., Weinhaus, B., Filla, M.S., and Peters, D.M. (2019a). Genomic/proteomic analyses of dexamethasone-treated human trabecular meshwork cells reveal a role for GULP1 and ABR in phagocytosis. Mol Vis *25*, 237-254.
21. Faralli, J.A., Filla, M.S., and Peters, D.M. (2019b). Role of Fibronectin in Primary Open Angle Glaucoma. Cells *8*.
22. Fautsch, M.P., Howell, K.G., Vrabel, A.M., Charlesworth, M.C., Muddiman, D.C., and Johnson, D.H. (2005). Primary trabecular meshwork cells incubated in human aqueous humor differ from cells incubated in serum supplements. Invest Ophthalmol Vis Sci *46*, 2848-2856.
23. Fernández-Durango, R., Fernández-Martínez, A., García-Feijoo, J., Castillo, A., de la Casa, J.M., García-Bueno, B., Pérez-Nievas, B.G., Fernández-Cruz, A., and Leza, J.C. (2008). Expression of nitrotyrosine and oxidative consequences in the trabecular meshwork of patients with primary open-angle glaucoma. Invest Ophthalmol Vis Sci *49*, 2506-2511.
24. Filla, M.S., Meyer, K.K., Faralli, J.A., and Peters, D.M. (2021). Overexpression and Activation of αvβ3 Integrin Differentially Affects TGFβ2 Signaling in Human Trabecular Meshwork Cells. Cells *10*.
25. Fleenor, D.L., Shepard, A.R., Hellberg, P.E., Jacobson, N., Pang, I.H., and Clark,

A.F. (2006). TGFbeta2-induced changes in human trabecular meshwork: implications for intraocular pressure. Investigative ophthalmology & visual science *47*, 226-234.

26. Flügel-Koch, C., Ohlmann, A., Fuchshofer, R., Welge-Lüssen, U., and Tamm, E.R. (2004). Thrombospondin-1 in the trabecular meshwork: localization in normal and glaucomatous eyes, and induction by TGF-beta1 and dexamethasone in vitro. Exp Eye Res *79*, 649-663.
27. Förstermann, U., and Li, H. (2011). Therapeutic effect of enhancing endothelial nitric oxide synthase (eNOS) expression and preventing eNOS uncoupling. Br J Pharmacol *164*, 213-223.
28. Freedman, J., and Iserovich, P. (2013). Pro-Inflammatory Cytokines in Glaucomatous Aqueous and Encysted Molteno Implant Blebs and Their Relationship to Pressure. Invest Ophthalmol Vis Sci *54*, 4851-4855.
29. Fu, H., Siggs, O.M., Knight, L.S., Staffieri, S.E., Ruddle, J.B., Birsner, A.E., Collantes, E.R., Craig, J.E., Wiggs, J.L., and D'Amato, R.J. (2022). Thrombospondin 1 missense alleles induce extracellular matrix protein aggregation and TM dysfunction in congenital glaucoma. J Clin Invest *132*.
30. Galassi, F., Renieri, G., Sodi, A., Ucci, F., Vannozzi, L., and Masini, E. (2004). Nitric oxide proxies and ocular perfusion pressure in primary open angle glaucoma. Br J Ophthalmol *88*, 757-760.
31. Gao, Q., Chen, K., Gao, L., Zheng, Y., and Yang, Y.G. (2016). Thrombospondin-1 signaling through CD47 inhibits cell cycle progression and induces senescence in endothelial cells. Cell Death Dis *7*, e2368.
32. Ghimire, K., Li, Y., Chiba, T., Julovi, S.M., Li, J., Ross, M.A., Straub, A.C., O'Connell, P.J., Rüegg, C., Pagano, P.J., Isenberg, J.S., and Rogers, N.M. (2020). CD47 Promotes Age-Associated Deterioration in Angiogenesis, Blood Flow and Glucose Homeostasis. Cells *9*, 1695.
33. Haddadin, R.I., Oh, D.J., Kang, M.H., Villarreal, G., Jr., Kang, J.H., Jin, R., Gong, H., and Rhee, D.J. (2012). Thrombospondin-1 (TSP1)-null and TSP2-null mice exhibit lower intraocular pressures. Invest Ophthalmol Vis Sci *53*, 6708-6717.
34. Hill, L.J., Mead, B., Thomas, C.N., Foale, S., Feinstein, E., Berry, M., Blanch, R.J., Ahmed, Z., and Logan, A. (2018). TGF-β-induced IOP elevations are mediated by RhoA in the early but not the late fibrotic phase of open angle glaucoma. Mol Vis *24*, 712-726.
35. Honjo, M., and Tanihara, H. (2018). Impact of the clinical use of ROCK inhibitor on the pathogenesis and treatment of glaucoma. Jpn J Ophthalmol *62*, 109-126.
36. Hua, Y., Voorhees, A.P., and Sigal, I.A. (2018). Cerebrospinal Fluid Pressure: Revisiting Factors Influencing Optic Nerve Head Biomechanics. Invest Ophthalmol Vis Sci *59*, 154-165.
37. Isenberg, J.S., Frazier, W.A., and Roberts, D.D. (2008a). Thrombospondin-1: a physiological regulator of nitric oxide signaling. Cell Mol Life Sci *65*, 728-742.

38. Isenberg, J.S., Hyodo, F., Matsumoto, K., Romeo, M.J., Abu-Asab, M., Tsokos, M., Kuppusamy, P., Wink, D.A., Krishna, M.C., and Roberts, D.D. (2007). Thrombospondin-1 limits ischemic tissue survival by inhibiting nitric oxide-mediated vascular smooth muscle relaxation. Blood *109*, 1945-1952.
39. Isenberg, J.S., Maxhimer, J.B., Hyodo, F., Pendrak, M.L., Ridnour, L.A., DeGraff, W.G., Tsokos, M., Wink, D.A., and Roberts, D.D. (2008b). Thrombospondin-1 and CD47 limit cell and tissue survival of radiation injury. The American journal of pathology *173*, 1100-1112.
40. Joe, M.K., Sohn, S., Kim, T.E., Im, J.E., Choi, Y.R., and Kee, C. (2011). Analysis of glucocorticoid-induced MYOC expression in human trabecular meshwork cells. Vision Res *51*, 1033-1038.
41. Julovi, S.M., Sanganeria, B., Minhas, N., Ghimire, K., Nankivell, B., and Rogers, N.M. (2020). Blocking thrombospondin-1 signaling via CD47 mitigates renal interstitial fibrosis. Lab Invest *100*, 1184-1196.
42. Kale, A., Rogers, N.M., and Ghimire, K. (2021). Thrombospondin-1 CD47 Signalling: From Mechanisms to Medicine. Int J Mol Sci *22*.
43. Kampougeris, G., Spyropoulos, D., and Mitropoulou, A. (2013). Intraocular Pressure rise after Anti-VEGF Treatment: Prevalence, Possible Mechanisms and Correlations. J Curr Glaucoma Pract *7*, 19-24.
44. Keller, K.E., Bhattacharya, S.K., Borrás, T., Brunner, T.M., Chansangpetch, S., Clark, A.F., Dismuke, W.M., Du, Y., Elliott, M.H., Ethier, C.R., Faralli, J.A., Freddo, T.F., Fuchshofer, R., Giovingo, M., Gong, H., Gonzalez, P., Huang, A., Johnstone, M.A., Kaufman, P.L., Kelley, M.J., Knepper, P.A., Kopczynski, C.C., Kuchtey, J.G., Kuchtey, R.W., Kuehn, M.H., Lieberman, R.L., Lin, S.C., Liton, P., Liu, Y., Lütjen-Drecoll, E., Mao, W., Masis-Solano, M., McDonnell, F., McDowell, C.M., Overby, D.R., Pattabiraman, P.P., Raghunathan, V.K., Rao, P.V., Rhee, D.J., Chowdhury, U.R., Russell, P., Samples, J.R., Schwartz, D., Stubbs, E.B., Tamm, E.R., Tan, J.C., Toris, C.B., Torrejon, K.Y., Vranka, J.A., Wirtz, M.K., Yorio, T., Zhang, J., Zode, G.S., Fautsch, M.P., Peters, D.M., Acott, T.S., and Stamer, W.D. (2018). Consensus recommendations for trabecular meshwork cell isolation, characterization and culture. Exp Eye Res *171*, 164-173.
45. Kim, M.H., and Lim, S.H. (2022). Matrix Metalloproteinases and Glaucoma. Biomolecules *12*.
46. Kondkar, A.A., Sultan, T., Almobarak, F.A., Kalantan, H., Al-Obeidan, S.A., and Abu-Amero, K.K. (2018). Association of increased levels of plasma tumor necrosis factor alpha with primary open-angle glaucoma. Clin Ophthalmol *12*, 701-706.
47. Kuchtey, J., Kunkel, J., Burgess, L.G., Parks, M.B., Brantley, M.A., Jr., and Kuchtey, R.W. (2014). Elevated transforming growth factor β1 in plasma of primary open-angle glaucoma patients. Invest Ophthalmol Vis Sci *55*, 5291-5297.
48. Lamy, L., Ticchioni, M., Rouquette-Jazdanian, A.K., Samson, M., Deckert, M., Greenberg, A.H., and Bernard, A. (2003). CD47 and the 19 kDa interacting protein-

3 (BNIP3) in T cell apoptosis. J Biol Chem *278*, 23915-23921.
49. Lawler, J.W., Slayter, H.S., and Coligan, J.E. (1978). Isolation and characterization of a high molecular weight glycoprotein from human blood platelets. J Biol Chem *253*, 8609-8616.
50. Lee, J., Choi, J.A., Ju, H.-h., Kim, J.-E., Paik, S.-Y., and Rao, P.V. (2021). Role of MCP-1 and IL-8 in viral anterior uveitis, and contractility and fibrogenic activity of trabecular meshwork cells. Scientific Reports *11*, 14950.
51. Li, T., Lindsley, K., Rouse, B., Hong, H., Shi, Q., Friedman, D.S., Wormald, R., and Dickersin, K. (2016). Comparative Effectiveness of First-Line Medications for Primary Open-Angle Glaucoma: A Systematic Review and Network Meta-analysis. Ophthalmology *123*, 129-140.
52. Liu, X., Wu, Z., Sheibani, N., Brandt, C.R., Polansky, J.R., and Kaufman, P.L. (2003). Low dose latrunculin-A inhibits dexamethasone-induced changes in the actin cytoskeleton and alters extracellular matrix protein expression in cultured human trabecular meshwork cells. Experimental Eye Research *77*, 181-188.
53. Logie, J.J., Ali, S., Marshall, K.M., Heck, M.M., Walker, B.R., and Hadoke, P.W. (2010). Glucocorticoid-mediated inhibition of angiogenic changes in human endothelial cells is not caused by reductions in cell proliferation or migration. PLoS One *5*, e14476.
54. Ma, D., Liu, S., Lal, B., Wei, S., Wang, S., Zhan, D., Zhang, H., Lee, R.S., Gao, P., Lopez-Bertoni, H., Ying, M., Li, J.J., Laterra, J., Wilson, M.A., and Xia, S. (2019). Extracellular Matrix Protein Tenascin C Increases Phagocytosis Mediated by CD47 Loss of Function in Glioblastoma. Cancer Res *79*, 2697-2708.
55. Manna, P.P., and Frazier, W.A. (2003). The mechanism of CD47-dependent killing of T cells: heterotrimeric Gi-dependent inhibition of protein kinase A. J Immunol *170*, 3544-3553.
56. McDonnell, F., Perkumas, K.M., Ashpole, N.E., Kalnitsky, J., Sherwood, J.M., Overby, D.R., and Stamer, W.D. (2020). Shear Stress in Schlemm's Canal as a Sensor of Intraocular Pressure. Scientific Reports *10*, 5804.
57. Moretti, L., Stalfort, J., Barker, T.H., and Abebayehu, D. (2022). The interplay of fibroblasts, the extracellular matrix, and inflammation in scar formation. J Biol Chem *298*, 101530.
58. Murphy-Ullrich, J.E., and Downs, J.C. (2015). The Thrombospondin1-TGF-β Pathway and Glaucoma. J Ocul Pharmacol Ther *31*, 371-375.
59. Obazawa, M., Mashima, Y., Sanuki, N., Noda, S., Kudoh, J., Shimizu, N., Oguchi, Y., Tanaka, Y., and Iwata, T. (2004). Analysis of porcine optineurin and myocilin expression in trabecular meshwork cells and astrocytes from optic nerve head. Invest Ophthalmol Vis Sci *45*, 2652-2659.
60. Okunuki, Y., Tabor, S.J., Lee, M.Y., and Connor, K.M. (2021). CD47 Deficiency Ameliorates Ocular Autoimmune Inflammation. Front Immunol *12*, 680568.
61. Patel, P.D., Chen, Y.L., Kasetti, R.B., Maddineni, P., Mayhew, W., Millar, J.C., Ellis,

D.Z., Sonkusare, S.K., and Zode, G.S. (2021). Impaired TRPV4-eNOS signaling in trabecular meshwork elevates intraocular pressure in glaucoma. Proc Natl Acad Sci U S A *118*.

62. Peters, J.C., Bhattacharya, S., Clark, A.F., and Zode, G.S. (2015). Increased Endoplasmic Reticulum Stress in Human Glaucomatous Trabecular Meshwork Cells and Tissues. Invest Ophthalmol Vis Sci *56*, 3860-3868.
63. Polansky, J.R., Fauss, D.J., and Zimmerman, C.C. (2000). Regulation of TIGR/MYOC gene expression in human trabecular meshwork cells. Eye (London, England) *14 (Pt 3B)*, 503-514.
64. Quigley, H.A. (1999). Neuronal death in glaucoma. Progress in retinal and eye research *18*, 39-57.
65. Reina-Torres, E., De Ieso, M.L., Pasquale, L.R., Madekurozwa, M., van Batenburg-Sherwood, J., Overby, D.R., and Stamer, W.D. (2021). The vital role for nitric oxide in intraocular pressure homeostasis. Prog Retin Eye Res *83*, 100922.
66. Ridnour, L.A., Isenberg, J.S., Espey, M.G., Thomas, D.D., Roberts, D.D., and Wink, D.A. (2005). Nitric oxide regulates angiogenesis through a functional switch involving thrombospondin-1. Proceedings of the National Academy of Sciences *102*, 13147-13152.
67. Roberts, D.D., and Isenberg, J.S. (2021). CD47 and thrombospondin-1 regulation of mitochondria, metabolism, and diabetes. Am J Physiol Cell Physiol *321*, C201-c213.
68. Rogers, N.M., Thomson, A.W., and Isenberg, J.S. (2012). Activation of parenchymal CD47 promotes renal ischemia-reperfusion injury. J Am Soc Nephrol *23*, 1538-1550.
69. Saumet, A., Slimane, M.B., Lanotte, M., Lawler, J., and Dubernard, V. (2005). Type 3 repeat/C-terminal domain of thrombospondin-1 triggers caspase-independent cell death through CD47/alphavbeta3 in promyelocytic leukemia NB4 cells. Blood *106*, 658-667.
70. Schlunck, G., Meyer-ter-Vehn, T., Klink, T., and Grehn, F. (2016). Conjunctival fibrosis following filtering glaucoma surgery. Exp Eye Res *142*, 76-82.
71. Schneemann, A., Leusink-Muis, A., van den Berg, T., Hoyng, P.F., and Kamphuis, W. (2003). Elevation of nitric oxide production in human trabecular meshwork by increased pressure. Graefe's archive for clinical and experimental ophthalmology = Albrecht von Graefes Archiv fur klinische und experimentelle Ophthalmologie *241*, 321-326.
72. Schuster, A.K., Erb, C., Hoffmann, E.M., Dietlein, T., and Pfeiffer, N. (2020). The Diagnosis and Treatment of Glaucoma. Dtsch Arztebl Int *117*, 225-234.
73. Shan, S.W., Do, C.W., Lam, T.C., Kong, R.P.W., Li, K.K., Chun, K.M., Stamer, W.D., and To, C.H. (2017). New Insight of Common Regulatory Pathways in Human Trabecular Meshwork Cells in Response to Dexamethasone and Prednisolone Using an Integrated Quantitative Proteomics: SWATH and MRM-HR Mass Spectrometry. Journal of Proteome Research *16*, 3753-3765.
74. Sharma, A., Patil, A.J., Mansoor, S., Estrago-Franco, M.F., Raymond, V., Kenney,

M.C., and Kuppermann, B.D. (2013). Effects of dexamethasone on human trabecular meshwork cells in vitro. Graefes Arch Clin Exp Ophthalmol *251*, 1741-1746.

75. Shifera, A.S., Trivedi, S., Chau, P., Bonnemaison, L.H., Iguchi, R., and Alvarado, J.A. (2010). Constitutive secretion of chemokines by cultured human trabecular meshwork cells. Experimental eye research *91*, 42-47.
76. Sierra, A., Navascués, J., Cuadros, M.A., Calvente, R., Martín-Oliva, D., Ferrer-Martín, R.M., Martín-Estebané, M., Carrasco, M.C., and Marín-Teva, J.L. (2014). Expression of inducible nitric oxide synthase (iNOS) in microglia of the developing quail retina. PLoS One *9*, e106048.
77. Smith, D.W., Lee, C.J., and Gardiner, B.S. (2020). No flow through the vitreous humor: How strong is the evidence? Prog Retin Eye Res, 100845.
78. Soh, Z., Yu, M., Betzler, B.K., Majithia, S., Thakur, S., Tham, Y.C., Wong, T.Y., Aung, T., Friedman, D.S., and Cheng, C.Y. (2021). The Global Extent of Undetected Glaucoma in Adults: A Systematic Review and Meta-analysis. Ophthalmology *128*, 1393-1404.
79. Soto-Pantoja, D.R., Stein, E.V., Rogers, N.M., Sharifi-Sanjani, M., Isenberg, J.S., and Roberts, D.D. (2013). Therapeutic opportunities for targeting the ubiquitous cell surface receptor CD47. Expert Opin Ther Targets *17*, 89-103.
80. Stamer, W.D., and Clark, A.F. (2017). The many faces of the trabecular meshwork cell. Exp Eye Res *158*, 112-123.
81. Steely, H.T., Browder, S.L., Julian, M.B., Miggans, S.T., Wilson, K.L., and Clark, A.F. (1992). The effects of dexamethasone on fibronectin expression in cultured human trabecular meshwork cells. Invest Ophthalmol Vis Sci *33*, 2242-2250.
82. Stein, J.D., Khawaja, A.P., and Weizer, J.S. (2021). Glaucoma in Adults-Screening, Diagnosis, and Management: A Review. Jama *325*, 164-174.
83. Sun, M.H., Pang, J.H., Chen, S.L., Han, W.H., Ho, T.C., Chen, K.J., Kao, L.Y., Lin, K.K., and Tsao, Y.P. (2010). Retinal protection from acute glaucoma-induced ischemia-reperfusion injury through pharmacologic induction of heme oxygenase-1. Invest Ophthalmol Vis Sci *51*, 4798-4808.
84. Sweetwyne, M.T., and Murphy-Ullrich, J.E. (2012). Thrombospondin1 in tissue repair and fibrosis: TGF-β-dependent and independent mechanisms. Matrix Biol *31*, 178-186.
85. Tamm, E.R. (2009). The trabecular meshwork outflow pathways: structural and functional aspects. Exp Eye Res *88*, 648-655.
86. Taurone, S., Ripandelli, G., Pacella, E., Bianchi, E., Plateroti, A.M., De Vito, S., Plateroti, P., Grippaudo, F.R., Cavallotti, C., and Artico, M. (2015). Potential regulatory molecules in the human trabecular meshwork of patients with glaucoma: Immunohistochemical profile of a number of inflammatory cytokines. Mol Med Rep *11*, 1384-1390.
87. Tripathi, R.C., Li, J., Chan, W.F., and Tripathi, B.J. (1994). Aqueous humor in glaucomatous eyes contains an increased level of TGF-beta 2. Exp Eye Res *59*, 723-

727.
88. Ulhaq, Z.S., Soraya, G.V., Budu, and Wulandari, L.R. (2020). The role of IL-6-174 G/C polymorphism and intraocular IL-6 levels in the pathogenesis of ocular diseases: a systematic review and meta-analysis. Scientific Reports *10*, 17453.
89. Vingolo, E.M., Chabib, A., and Anselmucci, F. (2019). Regeneration of trabecular meshwork in primary open angle glaucoma by stem cell therapy: a new treatment approach. Transplant Research and Risk Management *Volume 11*, 11-16.
90. Wang, B., Kasper, M., Laffer, B., Meyer Zu Hörste, G., Wasmuth, S., Busch, M., Jalilvand, T.V., Thanos, S., Heiligenhaus, A., Bauer, D., and Heinz, C. (2020). Increased Hydrostatic Pressure Promotes Primary M1 Reaction and Secondary M2 Polarization in Macrophages. Front Immunol *11*, 573955.
91. Wang Frau, B. (2020). Alteration in bone marrow derived macrophage and trabecular meshwork cell reactions under increased hydrostatic pressure.
92. Wang, S.K., Xue, Y., and Cepko, C.L. (2021). Augmentation of CD47/SIRPα signaling protects cones in genetic models of retinal degeneration. JCI Insight *6*.
93. Watanabe, M., Ida, Y., Ohguro, H., Ota, C., and Hikage, F. (2021). Establishment of appropriate glaucoma models using dexamethasone or TGFβ2 treated three-dimension (3D) cultured human trabecular meshwork (HTM) cells. Sci Rep *11*, 19369.
94. Wooff, Y., Man, S.M., Aggio-Bruce, R., Natoli, R., and Fernando, N. (2019). IL-1 Family Members Mediate Cell Death, Inflammation and Angiogenesis in Retinal Degenerative Diseases. Front Immunol *10*, 1618.
95. Yang, R., Liu, Q., and Zhang, M. (2022). The Past and Present Lives of the Intraocular Transmembrane Protein CD36. Cells *12*.
96. Yao, M., Roberts, D.D., and Isenberg, J.S. (2011). Thrombospondin-1 inhibition of vascular smooth muscle cell responses occurs via modulation of both cAMP and cGMP. Pharmacol Res *63*, 13-22.
97. Yemanyi, F., Baidouri, H., Burns, A.R., and Raghunathan, V. (2020). Dexamethasone and Glucocorticoid-Induced Matrix Temporally Modulate Key Integrins, Caveolins, Contractility, and Stiffness in Human Trabecular Meshwork Cells. Invest Ophthalmol Vis Sci *61*, 16.
98. Yun, H., Zhou, Y., Wills, A., and Du, Y. (2016). Stem Cells in the Trabecular Meshwork for Regulating Intraocular Pressure. J Ocul Pharmacol Ther *32*, 253-260.
99. Zhang, W., Huang, Q., Xiao, W., Zhao, Y., Pi, J., Xu, H., Zhao, H., Xu, J., Evans, C.E., and Jin, H. (2020). Advances in Anti-Tumor Treatments Targeting the CD47/SIRPα Axis. Front Immunol *11*, 18.
100. Zhu, J.D., Xie, L.L., Li, Z.Y., and Lu, X.H. (2019). The prognosis of trabeculectomy in primary angle-closure glaucoma patients. Int J Ophthalmol *12*, 66-72.

8 List of Figures and Tables

Figures

Tables

9 List of Abbreviations

Abbreviations	Full name
AC	anterior chamber
ACG	angle-closure glaucoma
ACG	angle-closure glaucoma
AH	aqueous humor
Arg	arginase
BP	blood pressure
cAMP	cyclic adenosine monophosphate
CCL	chemokine ligand
CD	cluster of differentiation
cGMP	cyclic guanosine 3', 5'-monophosphate
CRT	calreticulin
CSFP	cerebrospinal fluid pressure
CXCL	chemokine ligand
Dex	dexamethasone
DMF	N, N-dimethylformamide
DMSO	demethylsulfoxid
EAU	experimental autoimmune uveitis
ECM	extracellular matrix
EDTA	ethylendiamintetraacetat
EGF	epidermal growth factor
EHP	elevated hydrostatic pressure
eNOS	endothelial nitric oxide synthase
FBS	Fetal Bovine Serum
FGF	fibroblast growth factor
GEO	gene expression omnibus

H_2SO_4	Sulfuric acid
HCL	hydrochloric acid
HTM	human trabecular meshwork
IF	immunofluorescence
IHC	immunohistochemistry
IL	interleukin
IOP	intraocular pressure
IRI	ischemia-reperfusion injury
LC	lamina cribrosa
LRP	lipoprotein receptor related protein
MCP	monocyte chemoattractant protein
MMPs	matrix metalloproteinases
MTT	3- (4,5-Dimethylthiazol-2-yl)-2,5-diphenyltetrazolium bromide
NaCl	Sodium chloride
NaHCO3	Sodium hydrogen carbonate
NaOH	Sodium hydroxide solution
NO	nitric oxide
NTG	normal-tension glaucoma
OAG	open-angle glaucoma
OBF	ocular blood flow
ONH	optic nerve hypoplasia
PACG	primary angle-closure glaucoma
PBS	Phosphate-buffered saline
Pen/Strep	Penicillin / Streptomycin
PFA	Paraformaldehyde
POAG	primary open angle glaucoma
PVDF	polyvinylidene difluoride

RGCs	retinal ganglion cells
ROS	reactive oxygen species
RP	retinitis pigmentosa
RT	room temperature
sGC	soluble guanylate cyclase
SIRPα	signal-regulatory protein alpha
TGF	transforming growth factor
TIMP	tissue inhibitors of metalloproteinase
TM	trabecular meshwork
TNF	tumor necrosis factor
TSP	thrombospondin
VEGF	vascular endothelial growth factor
WB	western blotting
α-SMA	alpha-smooth muscle actin

10 Acknowledgement

Finally arrived at this page. Looking back, the only sentiment that prevails is gratitude.

First and foremost, I extend my heartfelt appreciation to my supervisor Professor Heinz for his consistent and helpful support throughout my M.D. study. I would want to thank him for his patience, help, empathy, and academic professions. He provided me with excellent chances and advice in writing research papers, and he also spent significant amount of time reviewing my thesis and providing me with constructive feedback to help me better my work. I consider myself incredibly fortunate to have benefited from his mentorship, without which the completion of my thesis would have been an insurmountable challenge. His encouragement has been a constant source of motivation.

I would like to express my gratitude to Dr. Dirk Bauer. He was the first to propose this research and played a pivotal role in designing this thesis. His guidance from the basics of cell cultivation to invaluable assistance during experiments has been crucial to the development of my research. Special thanks to Dr. Maren Kasper for her teachings on flow cytometry and cultivating good experimental practices. I would also thank to Melanie Schell, with whom I consistently exchanged encouragement and shared valuable experimental insights. Professor Heiligenhaus and Dr. Karoline Baquet-Walscheid shared their both experimental and clinical experiences has been invaluable to my study. The knowledge gained during our participation in the journal club has been particularly enlightening.

I am grateful to everyone I encountered in the laboratory; our shared birthday celebrations created a warm and familial atmosphere that made my academic journey even more memorable. Special thanks also go to the members I met at St. Franziskus Hospital for their contributions to my learning and overall experience.

I express sincere gratitude to Professor Yanning Yang, my master's thesis supervisor, for providing the foundational guidance that has greatly contributed to my M.D. study. My

heartfelt thanks also go to friends both in Germany and China, whose companionship, shared holidays, and travel adventures have added vibrant colors to my life.

To my homeland, China, and the support of the China Scholarship Council (CSC), I extend my sincere gratitude for their contributions to my study.

Lastly, I express gratitude to my loving parents who respect my adult decisions, provide the support of a child, and steadfastly propel my steps forward on this distant journey. They are the beacon that forever leaves a light for me to rest.

In the words of a Chinese poem, "My little boat passes by ten thousand peaks. The long journey ahead is both vast and brilliant". (轻舟已过万重山，长路漫漫亦灿灿). This is not just the end of a chapter but the beginning of a new one. Thank you to everyone who has been part of this incredible journey. Vielen Dank. 谢谢！

11 Curriculum Vitae

This curriculum vitae is not included in the online version for data protection reasons.